DOI:10.14753/SE.2024.3024

SEMMELWEIS EGYETEM

DOKTORI ISKOLA

Ph.D. értekezések

3024.

CSŐRE JUDIT

Szív- és érrendszeri betegségek élettana és klinikuma
című program

Programvezető: Dr. Merkely Béla, egyetemi tanár

Témavezető: Dr. Csobay-Novák Csaba, egyetemi adjunktus

DOI:10.14753/SE.2024.3024

ADVANCES IN MAGNETIC RESONANCE IMAGING OF PERIPHERAL ARTERIAL DISEASE: NON-CONTRAST MAGNETIC RESONANCE ANGIOGRAPHY AND ARTIFICIAL INTELLIGENCE-AIDED PLAQUE ANALYSIS

PhD thesis

Judit Csőre MD

Cardiovascular Medicine and Research Division

Semmelweis University Doctoral School

Supervisor:	Csaba Csobay-Novák, MD, PhD
Official reviewers:	Andrea Trajtler, MD, PhD
	Márton Tibor Berczeli MD, PhD
Complex Examination Committee:	
Head:	Tivadar Tulassay MD, DSc
Members:	Henriette Farkas MD, DSc
	Charaf Hassan, DSc

Budapest

2024

DOI:10.14753/SE.2024.3024

Table of Contents

DOI:10.14753/SE.2024.3024

List of abbreviations

2D: two-dimensional
3D: three-dimensional
ABI: ankle-brachial index
AHA: American Heart Association
ACC: American College of Cardiology
AP: ankle pressure
ASL: arterial spin-labeling
BASIL: “Bypass versus Angioplasty in Severe Ischaemia of the Leg”
BEST-CLI: “Best Endovascular versus Best Surgical Therapy in Patients with CLTI”
BMI: body-mass index
BMT: best medical therapy
bSSFP: Balanced Steady-State Free Precession
BSX: bypass surgery
CAD: coronary artery disease
CDS: color Duplex sonography
CEMRA: contrast-enhanced magnetic resonance angiography
CI: confidence interval
CIN: contrast-induced nephropathy
CLI: chronic limb ischemia
CLTI: chronic limb-threatening ischemia
CNN: convolutional neural network
CO_2: carbon dioxide
CTO: chronic total occlusion
COPD: chronic obstructive pulmonary disease
CMPR: curved multiplanar reconstruction
CTA: computed tomography angiography
DE-CTA: dual-energy computed tomography angiography
DESS: Double Echo Steady State
DM: diabetes mellitus
DSA: digital subtraction angiography

DVA: digital variance angiography

DWI: diffusion-weighted imaging

ECG: electrocardiography

ED: erectile disfunction

ESC: European Society of Cardiology

ESVS: European Society of Vascular Surgery

FA: flip angle

FDA: Food and Drug Administration

FLASH: Fast Low-Angle Shot

FMH: familial hypercholesterinemia

FOV: field of view

FPS: frames per second

FSD: flow-sensitive dephasing

FSE: fast spin-echo

GBCA: gadolinium-based contrast agents

eGFR: (estimated) glomerular filtration rate

GLASS: Global Limb Anatomic Staging System

GRAPPA: Generalized Autocalibrating Partial Parallel Acquisition

GWAS: genome-wide association study

HDL: high-density lipoprotein

HIC: high-income countries

ICC: intra-class correlation coefficient

IDIR: inflow-dependent inversion-recovery

IQR: interquartile range

KDOQI: Kidney Disease Outcomes Quality Initiative

LDL: low-density lipoprotein

LEAD: lower extremity arterial disease

LMIC: low-income or middle-income countries

MIP: maximum intensity projection

MiRNA: micro ribonucleic acid

MPR: multiplanar reconstruction

MRA: magnetic resonance angiography

MRI: magnetic resonance imaging

NATIVE SPACE: NATIVE = Non-contrast Angiography of the Arteries and Veins; SPACE = Sampling Perfection with Application Optimized Contrast by using different flip angle Evolution

NEMRA: non-enhanced magnetic resonance angiography

NICE: National Institute for Health and Care Excellence

NIFTI: Neuroimaging Informatics Technology Initiative

NPV: negative predictive value

NSF: nephrogenic systemic fibrosis

PC: phase-contrast

PCCT: photon-counting computed tomography

PAD: peripheral arterial disease

PAI: peripheral arterial intervention

PETRA: Pointwise-Encoding Time Reduction with Radial Acquisition

PPV: positive predictive value

PVI: percutaneous vascular intervention

PVR: pulse volume recording

RF: radiofrequency

RGB: red-green-blue

RNA: ribonucleic acid

QISS MRA: Quiescent-Interval Single-Shot Magnetic Resonance Angiography

SBP: systolic blood pressure

SD: standard deviation

SNP: single nucleotide polymorphism

STIR: Short Tau Inversion Recovery

SVS: Society of Vascular Surgery

T1w: T1-weighted

T2w: T2-weighted

TASC: TransAntlantic Inter-Society Consensus for the Management of Peripheral Arterial Disease

TcPO2: transcutaneous pressure of oxygen

TE: echo time

TM: transmetatarsal

TOF: time-of-flight

TP: toe pressure

TR: repetition time

TrueFISP: True Fast Imaging with Steady-State Free Precession

TSE: turbo spin-echo

UK: United Kingdom

UnQISS: ungated radial quiescent-inflow single-shot

UTE: ultrashort echo time

VAE: variational autoencoder

WIfI: Wound (W), Ischemia (I) and foot Infection (“fI”) - WIfI classification

1. Introduction

1.1. Definition and terminology of lower extremity peripheral arterial disease

Lower extremity arterial disease (LEAD) is an atherosclerotic condition that causes inadequate blood supply and ischemia to the affected limb. The illness in international terminology is frequently referred to as peripheral arterial disease (PAD), although this nomenclature may also indicate the stenosis or occlusion of both upper- or lower-extremity arteries (1) or even extracranial carotid, vertebral, mesenteric and renal arteries (2). Nevertheless, despite the inconsistent jargon, we can state that these terms are generally interchangeable, and PAD, in everyday and scientific terms, primarily suggests the clinical manifestation of atherosclerosis that affects peripheral arteries within the lower extremities (3).

1.2. Epidemiology of peripheral arterial disease

PAD, despite its growing prevalence, mortality, and serious clinical outcomes, is still underdiagnosed and underrecognized. In 2013, Fowkes et al. reported in a systematic review that approximately 202 million people worldwide lived with PAD, almost 70% of them living in low-income or middle-income countries (LMIC), while in high-income countries (HIC) the prevalence of PAD was approximately 5% at 40 to 44 years of age and 12% at 70 to 74 years of age in both women and men (4). The Global Burden of Cardiovascular Diseases report also implies that the incidence of the disease has risen each year since 1990 (5), and Song et al. estimated that in 2015 238 million people were living with PAD, therefore the total number of people with PAD was estimated to have risen by 17% from 202 million in 2010. Although the prevalence was higher in high-income countries than in low- and middle-income countries (7.4% versus 5.1%), reflecting the population size, most individuals with PAD (72.9%) resided in low- and middle-income countries (4, 6). Following coronary artery disease (CAD) and stroke, PAD is the third leading cause of atherosclerotic morbidity (7). A review of 124 studies showed that PAD patients have a high risk of all-cause and cardiovascular mortality, and suggested that the risk of myocardial infarction or stroke for those living with this condition was at least similar or higher to the risk in patients with CAD (8). Given the increasing number of cases and mortality, early diagnosis and treatment of PAD is of

utmost importance to prevent serious complications. In addition, due to this upward trend in disease prevalence, the economic and societal burden of PAD would also be considerable; regardless of whether revascularization or primary amputation is chosen as the course of treatment, the requirement for multiple procedures and prolonged hospitalization leads to increasing healthcare-associated costs of treating PAD and its most severe form, chronic limb-threatening ischemia (CLTI) (9).

1.3. Risk factors

The risk of developing PAD is influenced by several factors including genetics, age, sex, comorbidities such as hypertension (HT), diabetes mellitus (DM), dyslipidemia, or external factors such as smoking.

Recent studies have revealed a high degree of heterogeneity in the genetic architecture of PAD. The heritability of PAD has been estimated to be moderate in these studies (10). Current efforts have identified single nucleotide polymorphisms (SNPs) associated with PAD in genome-wide association studies (GWAS) analyses (11). One of the key points of research in recent years is the involvement of micro ribonucleic acids (miRNAs), many of which have been discovered to be misregulated in PAD patients (12). Improved knowledge of the genetic basis for PAD would enable earlier illness detection and more thorough pathophysiology comprehension of the disease mechanisms, leading to novel, targeted molecular therapies.

International data shows that older age is one of the strongest risk factors for PAD. The meta-analysis of Song et al. insisted that the prevalence of the disease almost doubles every 20 years, from 4.85% in the 45-year-old age group to 9.16% in the 65-year-old population, and to 19.28% in the over-85 population. The AHA/ACC (AHA: American Heart Association, ACC: American College of Cardiology) 2016 PAD Guideline recommends screening for PAD in adults aged 65 years and above using the ankle-brachial index (ABI) (13). In contrast, the 2017 ESC/ESVS (ESC: European Society of Cardiology, ESVS: European Society of Vascular Surgery) Guideline (2) and the 2024 ESVS Clinical Practice Guidelines on the Management of Asymptomatic Lower Limb Peripheral Arterial Disease and Intermittent Claudication (14) does not provide specific recommendations regarding the age at which PAD screening should be initiated.

Until approximately the age of 60 to 70 years, males are known to have a higher risk of atherosclerotic diseases, such as CAD and stroke, compared to females of the same age (15). However, in the 2019 systematic review from Song et al. of 118 articles reporting findings from 33 countries, the prevalence of PAD in women was greater than in men for many age ranges, especially in LMCIs (6). While women may exhibit no symptoms or experience milder symptoms compared to men, they tend to present with a more advanced stage of CLTI (16). The observation that women may have a higher prevalence of PAD compared to men has caused concern due to notable disparity in awareness and attention given to PAD in women (17).

Hypertension is associated with all forms of cardiovascular disease, including PAD. However, the relative risk for developing PAD is less for hypertension than for diabetes or smoking (16). A 2012 United States study reported the population-attributable fraction of hypertension for PAD to be 41% (18). Framingham cohort study revealed an increased risk of intermittent claudication, ranging 2 to 4 times higher, in both men and women with HT (19, 20).

Epidemiological evidence confirms an association between diabetes and increased prevalence of peripheral arterial disease. The duration and severity of DM correlate with the incidence and extent of PAD (21). The Framingham study found that individuals who had both diabetes and symptoms of peripheral arterial disease exhibited more than a 2-fold increase in the incidence of coronary heart disease, stroke, and cardiac failure (22). Hospital-based studies have shown that PAD is 2 to 7 times more common in individuals with diabetes, compared to those without DM. The prevalence of PAD in people with diabetes ranges from 9% to 55% (23). Additionally, patients with DM and PAD are at a 4-fold higher risk of lower extremity amputation than those without DM (24) and more than 50% of all amputations occur in people with DM (25).

Moreover, diabetic vasculopathy can lead to diabetic kidney disease, characterized by glomerular damage and subsequent elevation in urine albumin excretion, a decrease in glomerular filtration rate (GFR), or both. This serious complication affects approximately 20% to 40% of all diabetics. It is important to note that the presence of diabetic kidney disease may impose limitations on certain diagnostic tests used for the evaluation of PAD (26).

Although there are well-established, prospective associations between elevated lipoprotein levels and the development of coronary and cerebrovascular disease, the role of dyslipidemia in the pathogenesis of PAD remains controversial. This suggests potential differences in the underlying mechanisms contributing to these diseases (27). PAD frequently occurs in individuals with familial hypercholesterolemia (FMH), contraindicating the notion that serum cholesterol plays no role in this condition (28, 29). Building on the findings of the Framingham study, Murabito et al. reported that those with a total cholesterol level of 6.18 mmol/dl or greater had a 1.2 times higher chance of developing PAD compared to those with normal blood lipid values (20). Furthermore, several studies have confirmed the protective effect of high-density lipoprotein (HDL) levels in PAD (30, 31).

Smoking is a significant modifiable risk factor for PAD and is associated with progressive limb morbidity and other adverse cardiovascular outcomes, showing a consistent and important dose-response relationship (32). Olin et al. identified smoking as an independent risk factor for PAD, increasing the risk by four times and raising the risk of amputation in patients with intermittent claudication by 30% (33).

1.4. Symptoms and classification of peripheral artery disease

1.4.1. Symptoms

Comprehensive patient history and thorough physical examination play a vital role in diagnosing PAD. During the physical assessment, healthcare providers carefully examine for pulse loss, audible bruits, cool and cyanotic skin, pallor, dependent rubor, muscle atrophy, pain on palpation, hair loss on the lower extremity, non-healing wounds, and signs of limb gangrene. These clinical findings provide valuable insights for diagnosing PAD (34).

Majority - an estimated 20 to 50% - of all PAD patients report minimal or no symptoms. A noteworthy finding by Diehm et al. was that asymptomatic patients had a similar risk of mortality compared to symptomatic patients with PAD. Additionally, both symptomatic and asymptomatic patients with PAD had significantly higher mortality rates compared to individuals without PAD (35). Hence, the 2024 ESVS Guidelines suggest considering targeted PAD screening using ankle-brachial index measurements, focusing on the lowest recorded ankle pressure, for individuals clinically asymptomatic

yet at an elevated risk of lower limb PAD (14). The absence of symptoms in PAD can be attributed to reduced physical activity or slower walking speeds employed to prevent ischemic symptoms. In some cases, signs of PAD may also go unnoticed due to altered pain perception, as observed in individuals with peripheral neuropathy associated with diabetes (23).

Claudication, observed in approximately 30-40% of PAD patients (36), refers to an exertional, typically cramping pain or discomfort in the lower extremity muscles that occurs during walking. The symptoms of claudication typically subside within 10 minutes of rest (37). The walking distance at which symptoms manifest is influenced by the severity of the condition (38).

Ischemic rest pain typically emerges in advanced stages of PAD and is commonly localized in the forefoot region. This type of pain is exacerbated when the patient is lying down and relieved when the affected limb is dependent (e.g. hanging the leg over the edge of the bed). Consequently, individuals with ischemic rest pain often have trouble sleeping and resort to positions that temporarily alleviate the discomfort. It is important to note that edema resulting from keeping the leg in a dependent position can occasionally be mistaken for venous thrombosis (39). Rest pain should also be associated with one or more abnormal hemodynamic parameters. These parameters may include a reduced ABI, decreased ankle pressure, reduced toe pressure, low transcutaneous pressure of oxygen (TcPO2), or flat/minimally pulsatile Doppler arterial waveforms. The presence of these aberrant hemodynamic parameters in conjunction with sustained rest pain is indicative of significant vascular pathology (40).

A significant proportion (approximately 47-60%) of patients with PAD experience pain that deviates from the typical exertional pattern (41). In these cases, the pain may occur at rest or may not be alleviated with rest alone. Such patients often have additional comorbidities such as musculoskeletal disorders or diabetes, yet they remain susceptible to functional impairment and a decline in mobility (42).

In the context of PAD, wounds develop on the skin of the lower extremities due to poor circulation of blood caused by narrowed arteries, resulting in tissue damage, slow healing of wounds, and increased amputation risk. These wounds, often called ischemic ulcers or arterial ulcers, can be painful, prone to infection, and may not heal properly without appropriate intervention (40).

1.4.2. Classification

Establishing a consistent grading system for patients enables the application of objective criteria in treatment planning and provides a baseline for clinical follow-up. Due to the diverse presentations of PAD, various classification schemes have been proposed in the literature. One such scheme was introduced by Fontaine et al. in 1952, offering a straightforward clinical classification for patients with chronic arterial disease of the lower extremities, which associates the symptoms and signs with PAD (Table 1) (43). Subsequently, in 1986, with a revised version in 1997, the Rutherford classification was published to establish reporting standards for lower extremity ischemia. This classification system added objective criteria to each clinical category, facilitating a more standardized approach for both chronic (Table 2) and acute lower limb symptoms (44). The Trans-Atlantic Inter-Society Consensus (TASC) Document on the Management of Peripheral Arterial Disease I and II (16, 45) and subsequent revisions have focused primarily on retaining the clinical descriptions of the Rutherford categories. Other classification systems, such as The Global Limb Anatomic Staging System (GLASS) for CLTI (46), or Bollinger scoring method (47), and SVS runoff scores (2) exist and may also be useful in clinical decision-making. It is important to acknowledge that symptoms may not always align consistently with the stages outlined in these classification systems. In 2013, the Society for Vascular Surgery introduced a new classification system for the at-risk lower extremity. This system takes into account three primary factors that influence the risk of limb amputation, ultimately aiding in therapeutic decision-making: Wound (W), Ischemia (I), and foot Infection ("fI") - called the WIfI classification (48). Although most validation studies indicate that these scoring systems have the potential to enhance treatment planning (49), each of them assesses lesion length, location, or clinical symptoms but does not account for the composition and complexity of target lesions.

Table 1: Fontaine classification of chronic lower extremity ischemia.

Fontaine classification	
Stage	**Clinical description**
I	Asypmtopmatic
IIa	Claudication distance > 200 m
IIb	Claudication disctance <200m
III	Ischemic rest pain
IVa	Limited gangrene or ulceration
IVb	Extensive gangrene or ulceration

Table 2: Classification of chronic lower extremity ischemia as in Rutherford et al. (44). (AP: ankle pressure; PVR: pulse volume recording; TP: toe pressure; TM: transmetatarsal)

Rutherford classification			
Grade	**Category**	**Clinical description**	**Objective criteria**
0	**0**	Asymptomatic	Normal treadmill or reactive hyperemia test
I	**1**	Mild claudication	Completes treadmill exercise; AP after exercise >50 mmHg but at least 20 mmHg lower than resting value
	2	Moderate claudication	Between categories 1 and 3
	3	Severe claudication	Cannot complete standard treadmill exercise *and* AP after exercise <50 mmHg
II	**4**	Ischemic rest pain	Resting AP <40 mmHg, flat or barely pulsatile ankle or metatarsal PVR; TP <30 mm Hg
III	**5**	Minor tissue loss	Resting AP <60 mmHg, ankle or metatarsal PVR flat or barely pulsatile; TP <40 mm Hg
	6	Severe tissue loss or gangrene extending above TM level	Same as category 5

1.5. Diagnostic approach for lower extremity peripheral arterial disease

Accurate diagnosis of PAD relies on a thorough evaluation of patient history and a meticulous physical examination. However, to ensure precise treatment planning, a combination of non-invasive and invasive imaging techniques is essential. In line with various guidelines, different diagnostic imaging modalities such as color Duplex sonography (CDS), computed tomography angiography (CTA), digital subtraction angiography (DSA), and magnetic resonance angiography (MRA) are considered reasonable for assessing the anatomical characteristics of PAD (13). These advanced imaging techniques provide a comprehensive understanding of lower extremity arterial disease, facilitating improved diagnosis and therapeutic decision-making. Yet, each modality possesses its own advantages and disadvantages. Practitioners must be mindful of these limitations and comprehend the strengths and weaknesses associated with each modality, particularly in different clinical scenarios related to the presentation of PAD.

1.5.1. Ankle-brachial index

ABI is a widely utilized, non-invasive, and cost-effective tool for evaluating the status of peripheral vasculature. This simple yet effective test serves as an initial screening tool for assessing peripheral vascular health and helps healthcare professionals identify individuals at risk for PAD or other vascular conditions. It involves calculating the ratio between the systolic blood pressure (SBP) in the lower extremity, specifically at the ankle, and the upper extremity, measured at the brachial artery. The normal reference range for ABI typically falls between 0.9 and 1.4, indicating a healthy vascular condition. Generally, a lower ABI value indicates a more severe case of PAD, with cutoffs of 0.9, 0.7, and 0.5 indicating mild, moderate, and severe underlying disease, respectively (2). An ABI >1.40 represents arterial stiffening (calcification) and is also associated with a higher risk of CV events and mortality (50). ABI presented to have a sensitivity of 90% and specificity of 98% in detecting PAD. Additionally, it provides valuable information about the approximate location of the stenosis within the arterial system (23). An index ≤0.90 is associated with more than doubling of the 10-year rates of coronary events, cardiovascular mortality, and total mortality (50). However, reliability of this test is limited: patients with diabetes or those who have calcified and non-compliant vessels may frequently exhibit falsely elevated ABI results (51). Considering this, the AHA/ACC 2016 guidelines for the management of PAD advised liberal: ABI testing in any patient with clinical symptoms indicative of PAD or aberrant vascular exam findings is optional (13).

1.5.2. Ultrasound diagnostics

Ultrasonography, specifically the utilization of B-mode and color-flow Doppler mode is a widely accepted and non-invasive diagnostic method for assessing PAD. This imaging technique offers a comprehensive evaluation of the vessel lumen, and general characteristics of vascular stenosis, including location, extent, and severity. Additionally, it provides valuable insights into arterial hemodynamics. CDS is particularly well-suited for screening individuals suspected of having PAD (52). It is also highly effective in evaluating focal lesions, monitoring the progress of vascular interventions, and assisting in the selection of the appropriate access approach (53, 54).

Still, diagnostic accuracy may be limited by the experience of the examining physician, anatomy, atypical hemodynamic patterns, and severe artifacts caused by extensive

calcification. Despite the extensive literature on assessing carotid plaque volume, histopathologic composition, and morphology using CDS (55, 56), determining the precise characteristics of lower extremity plaques, especially in smaller below-the-knee arteries, poses a challenge (57). Moreover, obtaining a comprehensive picture of the whole lower extremity is also time-consuming and often difficult to perform.

1.5.3. Digital subtraction angiography

1.5.3.1. Digital subtraction angiography using iodinated contrast material

Despite the inherently invasive nature and significant limitations, DSA using iodinated contrast material remains the gold standard for imaging of PAD. In addition to the ability to assess lumen patency, presence of collateralization, and quality of flow, the dual diagnostic and therapeutic role of DSA imaging is unique. Major limitations of conventional DSA include limited two-dimensional perspective, radiation, requirement for nephrotoxic contrast material, inability to evaluate total occlusions or vessel wall characteristics, and susceptibility to motion artifact. New technologies have been developed as adjuncts to DSA and catheter-based therapies to enhance the utility of DSA. Still, the use of DSA for diagnostic purposes has declined significantly in recent years. Despite the overall marginalization of this imaging modality, its use may still be justified in certain clinical scenarios: in cases of arterial stenosis in the below-the-knee region, extensive calcification and consequent "blooming" artifacts can severely limit the image quality of CTA images. Therefore, the use of DSA is still often essential in establishing a therapeutic plan, considering possible complications (58). A new technique based on kinetic radiographic imaging called digital variance angiography (DVA) consists of several, generally underexposed images instead of using a single, fully exposed image and provides better image quality and lower radiation exposure than traditionally used DSA (59).

1.5.3.2. Digital subtraction angiography using carbon dioxide contrast material

Individuals with diabetes and accompanying renal failure are at an elevated risk for PAD, underscoring the importance of employing nephroprotective imaging techniques for diagnosis. Carbon dioxide (CO_2) digital subtraction angiography stands out as a well-established imaging method for interventions for evaluating lower extremity PAD and is recognized as a reference standard, primarily due to its excellent spatial resolution. in

those with impaired renal function and iodinated contrast hypersensitivity (60). CO_2 is an all-natural, non-toxic, negative contrast material, which is highly soluble in blood and is rapidly eliminated via the lungs. Still, as an invasive technique, it can lead to potential complications related to arterial puncture or exposure to ionizing radiation. Due to the low viscosity of CO_2, it is possible to use smaller angiographic catheters and improve the filling of severely diseased stenotic vessels. the primary concern when employing CO_2 as an intra-arterial contrast agent is the risk of air embolism. As a precaution against potential neurotoxicity and cardiac arrhythmia, CO_2 should not be administered above the diaphragm level. The complications of CO_2 DSA also include leg pain, abdominal pain, diarrhea, microvascular obstruction, and very rarely lethal complications such as nonobstructive mesenteric ischemia (61). Especially in the case of below-the-knee peripheral arterial interventions, CO_2 angiography may be associated with severe leg pain and consequent motion artifact (62). A higher frame rate per second is necessary to ensure sufficient image quality and prevent incomplete luminal filling caused by the breakup of CO_2 bubbles into smaller bubbles, which can mimic stenosis. However, achieving a higher frame rate requires a higher radiation dose. Also, the use of carbon dioxide is restricted in individuals with pulmonary hypertension and severe chronic obstructive pulmonary disease (COPD) (63).

1.5.4. Computed tomography angiography

CTA is an easily accessible and reproducible imaging technique that can evaluate lower extremity arteries from the abdominal region to the feet in a single scan, assisting both in the assessment of disease distribution and vascular morphology (64). This modality offers slightly lower spatial resolution than DSA with a short scan time and without the risks of an invasive procedure. The three-dimensional (3D) dataset allows further reconstruction of images such as volume rendered or maximum intensity projection (MIP) and curved multiplanar reconstructions (CMPR) (65). According to a meta-analysis of 70 studies, the pooled sensitivity and specificity of the modality for detecting stenosis of at least 50% per segment was 92% (66). Despite the challenges posed by "blooming" artifacts resulting from extensive calcification, as well as the potential risks associated with the use of iodinated contrast material and ionizing radiation, CTA remains a popular imaging modality for endovascular treatment planning, primarily due to its widespread availability and the relatively short duration of the examination (67). Future directions, such as Dual-

energy CTA (DE-CTA) and Photon-Counting CT (PCCT) can reduce "blooming" artifacts, offer more detailed tissue imaging, and possess high sensitivity for detecting vascular stenosis with a higher spatial resolution and lower radiation dose (68, 69).

1.5.5. Magnetic resonance imaging

1.5.5.1. Basic principles of magnetic resonance imaging

The significant progress in magnetic resonance imaging techniques has enabled the evaluation of PAD both with and without the need for contrast agents in a safe, non-invasive manner. Nevertheless, the complexity of interpreting images and understanding underlying physics can present challenges for physicians in terms of comprehension and utilization. Having a basic knowledge of the fundamental principles can facilitate wider acceptance and implementation of this technique in the assessment of PAD.

MRI machines operate by harnessing the interplay between the magnetic field, hydrogen ions (hydrogen nuclei or single protons, which are "spinning" (angular moment), and also "precessing" at a rate called Larmor frequency), and radiofrequency (RF) pulses. Placing a patient within an MRI magnetic field causes the alignment of the otherwise randomly oriented hydrogen ions in the tissues to orient in the same direction (parallel and antiparallel) as the magnetic field. By introducing an RF pulse that matches the Larmor frequency (i.e. at resonance) with specific settings generated by a transmit coil, the alignment of these protons can be altered. The duration from the RF excitation pulse to the data acquisition is referred to as the "echo time" (TE), while the duration between successive RF pulses is called the "repetition time" (TR). Once the RF pulse is deactivated, hydrogen nuclei strive to 1) realign with the magnetic field (called "realignment"), and 2) lose their resonance (called "dephasing" of protons) emitting a signal in the process. The intensity of this signal varies based on the specific tissue type (such as fat, muscle, or water) in which the protons are situated (Figure 1A) (70).

Taking the two basic types of MRI contrasts, "T1" and "T2", the so-called "T1" signal corresponds to the rate at which hydrogen ions realign, reflecting the length of time it takes for the longitudinal z-component (M_z) of tissue magnetization to regrowth to its initial maximum. Tissues characterized by short T1 relaxation times regain their equilibrium faster compared to those with longer T1 relaxation times. As a result, these tissues exhibit a brighter appearance on the MR image. On the other hand, T2 signal, associated with the hydrogen ion spin dephasing, is the length of time it takes for the

transverse components (M_{xy}) of magnetization to recover. When a substance has a short T2 relaxation time, its signal diminishes rapidly. As a result, substances with shorter T2 values seem darker compared to those with longer T2 values. Protons within tissues such as fat exhibit rapid realignment accompanied by high energy, resulting in a strong T1 signal. This phenomenon is utilized to create “T1-weighted” (T1w) images, TR can be optimized to achieve maximum T1 contrast. The dephasing of protons in water occurs at a relatively gradual pace, and this characteristic is utilized to generate “T2-weighted” (T2w) images that emphasize the presence of water (and also fat) within body tissues, in this case, TE can be optimized for maximum T2 contrast (Figure 1B). Other, specific, more complex MRI sequences or frequency-selective suppression pulses (e.g. diffusion-weighted (DWI) or Short Tau Inversion Recovery (STIR)) can be utilized to further evaluate different tissue types and characteristics and answer particular clinical questions. Using contrast material can alter the image signals in MRI by enhancing the differentiation between various tissues or highlighting specific areas of interest. These contrast materials typically contain paramagnetic (such as gadolinium) or superparamagnetic (such as iron oxide nanoparticles) substances that influence the relaxation times (T1 and T2) of nearby protons in the body. For T1w images, the contrast material shortens the T1 relaxation time of nearby tissues, resulting in increased signal intensity and better visualization of certain structures. For T2-weighted images, the contrast material lengthens the T2 relaxation time, leading to increased signal intensity and improved visibility of certain pathologies or abnormalities (71).

Upon acquiring MR signals, the raw data is preserved as an array of numerical values that correspond to spatial frequencies within the MR image, commonly referred to as "k-space". The central region of k-space carries details regarding image contrast, while the outer edges of k-space encode information about edge definition. Generally, enhancing spatial resolution necessitates sampling a greater number of points, leading to longer acquisition times.

MRI uses a strong magnetic field that can interact with metallic objects within the body. Patients with certain metallic implants or devices may be contraindicated for an MRI due to potential hazards. These include cardiac pacemakers, cochlear implants, certain types of aneurysm clips, some artificial heart valves, and neurostimulation devices. The presence of metallic fragments in the eyes or other vital organs is also a contraindication.

Additionally, MRI scanners can be small and confining, which can trigger claustrophobia in some individuals. Claustrophobia can cause severe anxiety and distress, making it difficult for patients to remain still during the procedure. In such cases, alternative imaging methods or sedation may be considered.

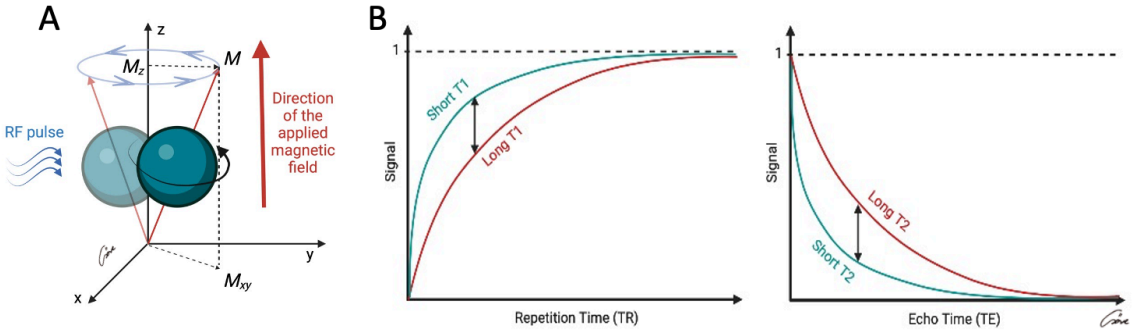

Figure 1: A) Individual, precessing hydrogen ion, placed in a strong magnetic field. After exciting a radiofrequency (RF) pulse, the proton aims to become aligned ("parallel") with the direction (or with the opposite direction, "antiparallel") of the magnetic field. Summation of longitudinal (Mz) and transverse (Mxy) magnetic moments gives the net magnetic vector (M) of the proton. The curved arrow represents the angular moment and the direction of the precession. B) Left: Tissues with short T1 relaxation time recover more quickly than those with long T1 relaxation time, producing a brighter spot on the MR image. T1 signal contrast is higher for lower repetition time (TR) values. Right: T2 reflects the length of time it takes for the MR signal to decay in the transverse plane. A short T2 means that the signal decays very rapidly. Consequently, substances with short T2 relaxation times appear darker than those with longer T2 values. Signal contrast can be increased by optimizing echo time (TE) values.

1.5.5.2. Contrast-enhanced magnetic resonance angiography

Contrast-enhanced magnetic resonance angiography (CEMRA) has shown high sensitivity and specificity when compared to both CTA and conventional DSA. One of the advantages of CEMRA is that it does not require the use of iodinated contrast material. CEMRA also offers superior soft tissue resolution, allowing for detailed visualization of anatomical structures (72). It has been demonstrated that CEMRA is a highly reliable method for visualizing and assessing the presence and extent of arterial narrowing or occlusion in patients with intermittent claudication and CLTI (Figure 2) (73). The imaging protocol used for capturing images of the peripheral vasculature from the aorta

down to the feet with high vessel-to-background contrast typically involves acquiring 3-4 sequential steps with an infusion rate of 0.1-0.2 mmol/kg (calculated based on the patient's weight) of contrast agent (74). Due to its exceptional soft tissue contrast, CEMRA also enables the evaluation of other, non-atherosclerotic vascular diseases which may be the underlying cause of intermittent claudication (e.g. vasculitis, cystic adventitial disease, popliteal entrapment, fibromuscular dysplasia, etc.) (75). An alternative method for CEMRA involves capturing multiple 3D volumes during the passage of a contrast agent bolus, employing a time-resolved acquisition technique, and providing a dynamic depiction of arterial and venous vasculature (Figure 3) (76).

However, certain factors may limit the use of CEMRA. Concerns have been raised regarding gadolinium-based contrast agents as a potential cause of nephrogenic systemic fibrosis in patients with renal dysfunction (especially with GFR<30ml/min) (77, 78). While there is still an ongoing debate regarding the safety of gadolinium use in this patient population, it appears that new-generation gadolinium-based contrast agents may offer a safer alternative (79). Awareness has also been raised regarding gadolinium retention in the brain, however, clear clinical correlation has not been identified yet (80). Alternatively, ferumoxytol, originally developed for iron-related treatments, could serve as a contrast material (81). While the number of clinical trials using ferumoxytol as a contrast agent is on the rise, it remains an off-label product for MRI applications.

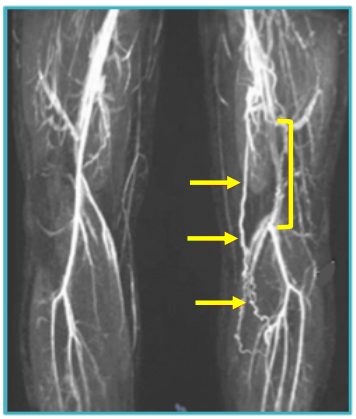

Figure 2: Contrast-enhanced magnetic resonance angiography of the femoropopliteal region. Coronal maximum intensity projection image shows the occlusion of the left superficial femoral artery (yellow bracket) and the resulting collateralization (yellow arrows).

DOI:10.14753/SE.2024.3024

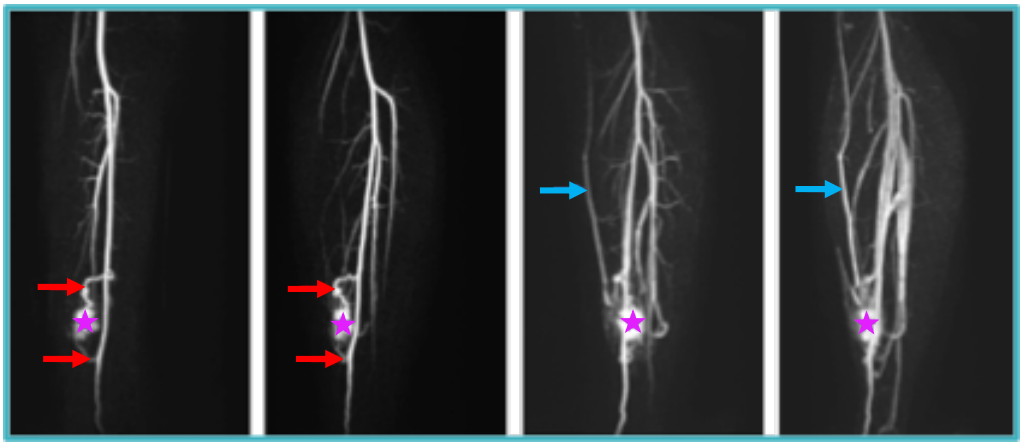

Figure 3: Dynamic, time-resolved three-dimensional contrast-enhanced magnetic resonance angiography of a calf arteriovenous malformation (purple asterisk). In the arterial phase (first two images), the presence of afferent arteries (red arrows) originating from the posterior tibial artery can be observed. In the third and fourth images, early filling of a superficial vein (blue arrows) is noticeable, which is attributed to a moderate arteriovenous shunt.

1.5.5.3. Non-enhanced magnetic resonance angiography

In recent decades, non-enhanced magnetic resonance angiography (NEMRA) techniques for imaging the peripheral arteries have undergone significant advancements. These imaging sequences offer several advantages, including the absence of ionizing radiation and the elimination of the need for contrast materials. Consequently, NEMRA is considered a safe imaging modality that can be repeated as needed without any associated risks (82).

NEMRA sequences can depict slow-flowing or even stationary blood and create nearly flow-independent angiograms where blood appears bright or dark (70). Black-blood magnetic resonance angiography techniques render flowing blood dark, which - in addition to quantitative measurements of lumen area - makes the evaluation of vessel wall easier (83). On the other hand, bright-blood NEMRA can evaluate flowing blood in the region of interest by using various sequences, such as balanced steady-state free-precession (bSSFP), phase-contrast (PC), subtractive fast spin-echo (FSE), arterial spin-labeling (ASL), inflow-dependent inversion-recovery (IDIR), time-of-flight (TOF), NATIVE SPACE (NATIVE = Non-contrast Angiography of the Arteries and Veins; SPACE = Sampling Perfection with Application Optimized Contrast by using different

flip angle Evolution), and Quiescent-Interval Single-Shot (QISS) MRA (82). Limitations (in addition to general MRI contraindications) may include long scan time and operator dependence; some sequences may only be suitable for small regions. Imaging of the entire lower extremity can be particularly difficult: as a number of PAD patients suffer from rest pain in lying position, severe artifacts can decrease the evaluability of lower extremity vasculature (84).

1.5.5.4. Quiescent-Interval Single-Shot Magnetic Resonance Angiography

QISS MRA is a novel, non-contrast protocol suitable for lower extremity peripheral arterial imaging both in 1.5T and 3T (85). Additionally, it showed promising results in the evaluation of other vascular pathologies such as abdominal aortic aneurysm or pulmonary embolism (86-88) This technique, compared with other NEMRA sequences such as NATIVE SPACE or FSE, had higher diagnostic performance and numerous advantages (89, 90). Conventional QISS MRA is based on TrueFISP ("True Fast Imaging with Steady-State Free Precession") measurements and bSSFP readout, which is capable of accurate and fast imaging of the entire lower extremity. The sequence begins with a pre-saturation step, utilizing a 90° RF pulse to saturate stationary tissues within the imaging slice. This is followed by a 90° venous suppression pulse. A "quiescent interval", synchronized with systole, allows for maximum inflow of unsaturated blood into the imaging slice. Subsequently, a fat saturation pulse is applied, and signal acquisition takes place during diastole using a two-dimensional (2D) bSSFP sequence. The entire process is then repeated until all required images are captured (91). The application of a single-shot acquisition with a very short (200–300 msec) period of data collection for each slice reduces the sensitivity to motion artifact (92) (Figure 4, 5). The images in the upper abdominal region are acquired in breath-hold to avoid respiratory artifacts. As a nonenhanced method for the assessment of PAD, QISS MRA had a high sensitivity (98.6%) and specificity (96%) for the detection of significant stenosis, using CEMRA as the reference standard (93). As QISS MRA evaluates flowing blood and not visualizing the vessel wall, it is also proved to be a reliable alternative to CTA, where sensitivity of QISS (95.83%) was significantly higher than that of CTA (74.19%) for heavily calcified segments with “blooming” artifact (94). QISS MRA also has a “push-button” setup

without the need for patient-specific adjustments, hence, the application of the protocol is easy and efficient for the imaging technologist.

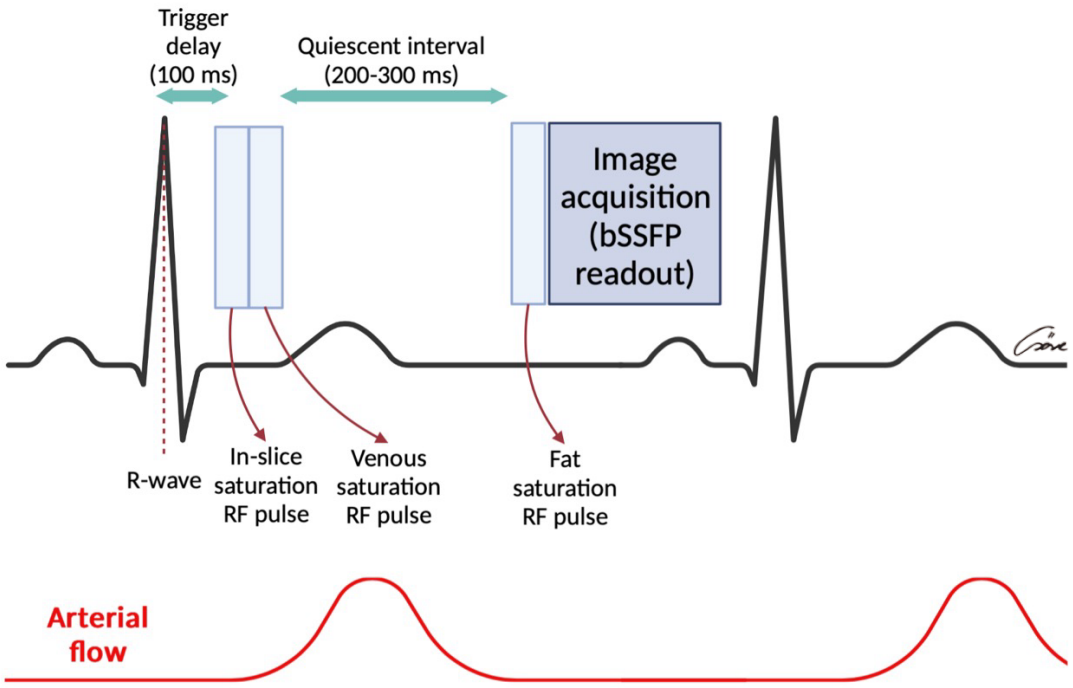

Figure 4: Quiescent-Interval Single-Shot sequence begins with a pre-saturation 90° RF pulse to saturate stationary tissues in the imaging slice. This is followed by a 90° venous suppression pulse. During a "quiescent interval" that coincides with systole, maximum unsaturated blood inflow into the imaging slice occurs. Subsequently, a fat saturation pulse is applied, and the signal is acquired during diastole using a two-dimensional (2D) bSSFP sequence. This process is repeated until all necessary images are captured. Using a single-shot acquisition with a very short (200–300 ms) data collection window for each slice minimizes sensitivity to motion artifacts. (bSSFP: balanced steady-state free precession)

DOI:10.14753/SE.2024.3024

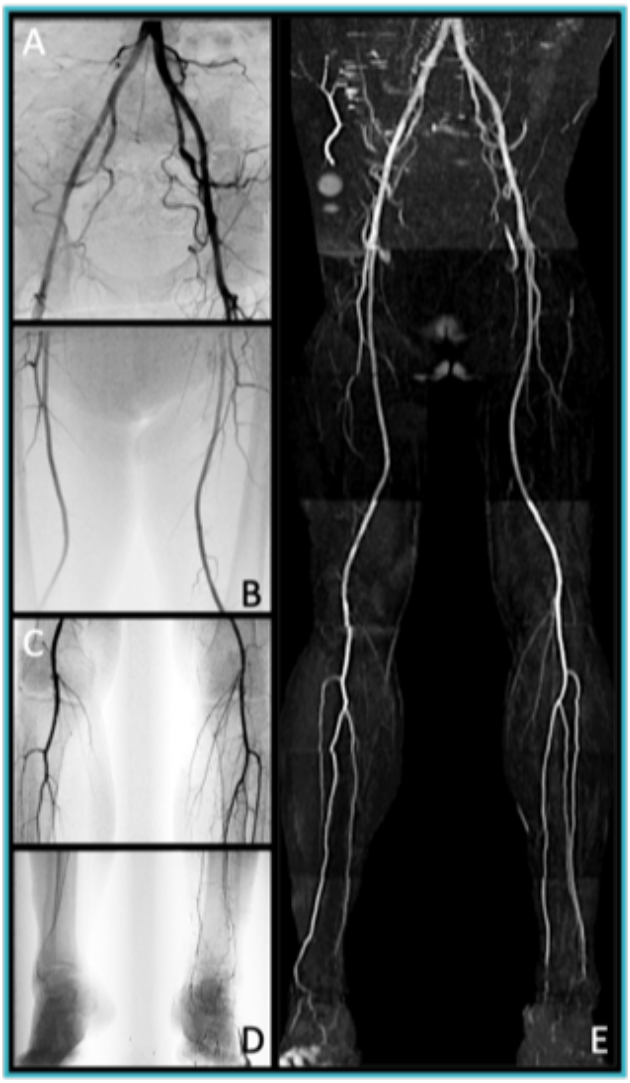

Figure 5: Comparison of iodinated contrast DSA (A, B, C, D) and Quiescent-Interval Single-Shot (E) images.

1.5.5.5. Magnetic resonance histology and plaque characterization

Due to its minimally invasive nature and low rate of periprocedural complications, percutaneous vascular intervention (PVI) is frequently selected as the primary treatment for PAD. Nevertheless, about 15-20% of patients experience immediate PVI failure, typically attributed to impenetrable plaques (95). Recent randomized controlled trials also showed that individuals necessitating bypass surgery following their initial PVI failure exhibit higher amputation rates and reduced long-term patency when compared to those who initially underwent bypass surgery utilizing autologous single-segment saphenous vein (96). The management of peripheral artery disease is constrained by existing imaging

techniques, as outlined earlier (97). One of the research priorities highlighted in the Global Vascular Guidelines by the Society for Vascular Surgery for critical limb-threatening ischemia is the enhancement of non-invasive PAD imaging through MRI (40). Until recently, the limited ability of MRI to accurately detect calcium deposits has hindered its widespread use for chronic total occlusion (CTO) applications. However, recent advancements in ultrashort echo time (UTE) MRI sequences have addressed this limitation. UTE sequences are capable of separating calcium from other tissues based on their distinct T2 relaxation time properties. By optimizing the echo time (UTE: TE ~ 20 ms) compared to conventional T2 sequences (TE ~ 40-100 ms), we can differentiate between calcium and other components, such as collagen, within different lesions (Figure 6). This breakthrough in MRI technology allows for improved characterization of PAD plaques and CTOs and may enhance the diagnostic and treatment capabilities in clinical practice (98-100). With the use of these state-of-the-art MRI sequences, lesions composed of “hard” (dense collagen and calcium) and “soft” tissue (loose fibrous tissue, microchannels, fat, thrombus) can easily be distinguished, showing calcium as hypointense, dense collagen as isointense and soft tissue as hyperintense relative to smooth muscle tissue signal (Figure 6 and 7).

Utilizing higher magnetic fields in MRI imaging can significantly enhance the resolution of acquired images, enabling us to identify more detailed plaque characteristics. For example, at 3T the isotropic resolution can be as high as 0.5 mm x 0.5 mm x 0.5 mm, while at 7T it can reach 0.2 mm x 0.2 mm x 0.2 mm in vivo. For excised plaque tissue at 9.4T, it is possible to achieve an even higher isotropic resolution of 0.156 mm x 0.156 mm x 0.156 mm. It is crucial to note that employing higher spatial resolutions at higher magnetic fields leads to longer acquisition times, potentially affecting patient comfort and workflow efficiency. Still, considering the aforementioned advantages of UTE contrast in differentiating plaque components, these sequences hold promise in facilitating PAD treatment planning and aiding in the selection of appropriate endovascular devices based on the specific tissue properties of the lesion (101).

DOI:10.14753/SE.2024.3024

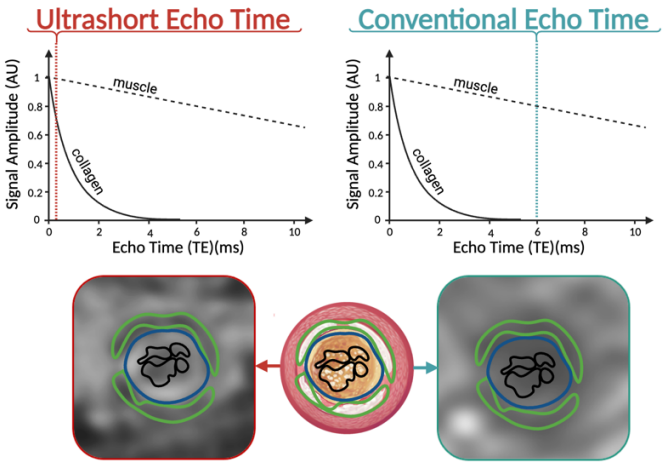

Figure 6: Signal behavior relationship to plaque composition in a chronic total occlusion. Signal decay times of dense collagen and muscle are as presented above. Ultrashort echo time images are acquired when dense collagen and muscle tissue still exhibit detectable signal. Conventional T2-weighted images are acquired after dense collagen (having a short T2 relaxation time) loses its signal and appears dark, compared with muscle that still retains signal. The images below illustrate a below-the-knee occlusion, composed of both concentric calcium (green outline, hypointense) and central, speckled calcium (black outline, hypointense) in a dense collagen matrix (blue outline, isointense).

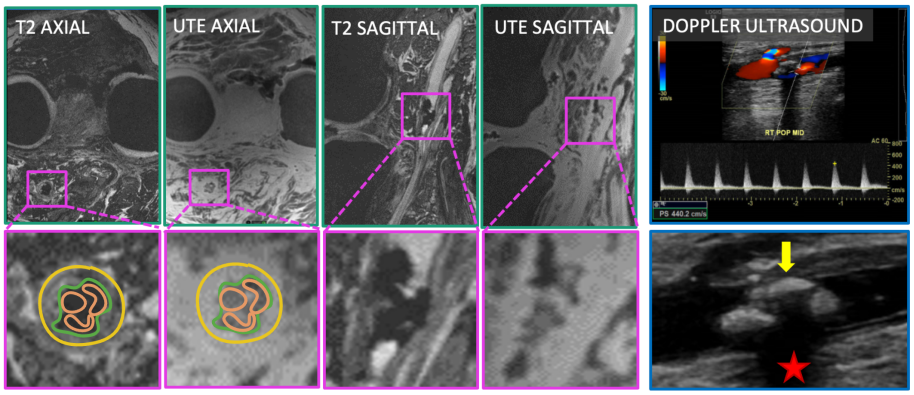

Figure 7: 7T magnetic resonance imaging and Doppler ultrasound of a popliteal artery plaque. On ultrasound images (right) an echogenic, nodular, calcified plaque (yellow arrow) with shadowing (red asterisk) causes significant hemodynamic stenosis (peak systolic velocity 440 m/s); detailed plaque morphology can be determined only to a very limited extent. 7T T2 and ultrashort echo time (UTE) images show explicit plaque structure with speckled calcium (orange outline, hypointense) in an isointense dense collagen matrix (green outline). Vessel lumen is outlined in yellow.

1.5.6. Application of artificial intelligence in medicine

1.5.6.1. Artificial intelligence in general

The term "Artificial Intelligence" (AI) was introduced by John McCarthy of Dartmouth College in 1956 and was also founded as an academic discipline. While there is ongoing debate among AI experts regarding the exact definitions of machine intelligence and machine learning, the general consensus is that AI encompasses advancements in computer hardware and software. These advancements aim to leverage, synthesize, and infer information to tackle problems, provide solutions, or generate new knowledge using algorithms or designs that are often inspired by human thinking and behavior, although they may not be identical (102).

1.5.6.2. Utilizing artificial intelligence in medical imaging

Advances in computer technology have also made the application of deep learning algorithms feasible for big data, such as medical image data. AI algorithms utilizing neural networks possess the capability to classify intricate data interrelationships in general (102-104). Specific AI algorithms transform information from medical image data into features using a dense representation, enabling unsupervised learning-based classifications. An example of such algorithms includes variational autoencoder (VAE), a type of generative deep learning algorithm, based on autoencoders which were originally introduced as self-organizing neural network models for pattern recognition with dimensionality reduction (105). VAEs, like other deep learning technologies, have found widespread application in medical image processing for many modalities including X-ray, CT, anatomical MRI, functional MRI, and PET (106-109). Due to this capability, VAEs are especially intriguing for their ability to condense complex MRI data into latent variables, aiming to construct an unsupervised classification algorithm for these values. This process results in a reduced-dimensional latent space, which has also found applications in medical imaging data (110, 111). VAEs for image processing consist of three main components. The encoder extracts and condenses the information into the latent space which the decoder then uses to reconstruct the original image, mirroring the steps used in the decoder in a reverse order (Figure 8). Both the encoder and the decoder are formed by 2D convolutional neural networks (2D CNNs) which were inspired by the architecture of human brain neurons. Modern neural networks extract image information

at different scales (112-114). The representation of the compressed data within the latent space can subsequently serve as a method for classifying the original images (115).

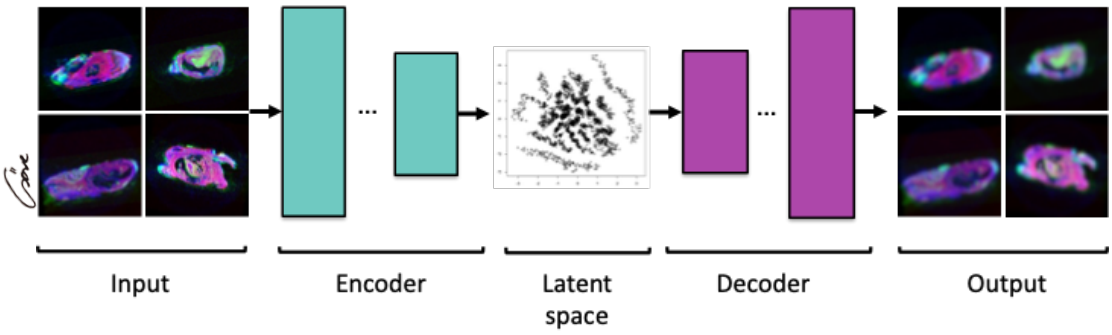

Figure 8: Schematic illustration of a variational autoencoder (VAE). In this configuration, magnetic resonance images of a tibial lesion are fed as input to the VAE. The encoder employs a series of operations to compress the information from the input images into two distinct numerical values within a latent space. Subsequently, the decoder utilizes the data from the latent space as input and generates output images that closely resemble the original input. This capability of the algorithm to produce output images resembling the input indicates its proficiency in classifying plaques.

1.5.6.3. AI-assisted plaque analysis using MRI datasets

Previously described innovative techniques in MRI are powerful, but their adoption in different clinical setups may be limited due to their complexity in interpretation. AI-assisted algorithms could potentially facilitate the interpretation process.

The successful training of the VAE algorithm necessitates the use of large amounts of data. For one MRI dataset, enough input images may be obtained through interpolated multiplanar reconstruction (MPR) of one lesion. The 2D image data may be created into a pseudo-color image where color components red, green, and blue are represented by the grayscale image values for the three (T1w, T2w and UTE) MRI contrast. These images will contain the two classes of interest which are intended to be distinguished, i.e. hard and soft tissue components, where the former will have little to no signal producing a black/dark image intensity while the signal of the latter will produce bright-colored regions. By effectively conducting a semi-supervised classification within the latent space, each lesion, represented by pseudo-color images, can be scored as predominantly composed of either hard or soft tissue. The presence or absence of these components has

previously been associated with the guidewire puncture force needed to navigate the lesion (101), potentially facilitating interventional procedure planning. In the future, AI-assisted plaque analysis may contribute to swift and precise assessments of lesion composition and crossability, thereby aiding clinical decision-making in PAD therapy.

1.6. Therapeutic approach

1.6.1. Prevention and best medical therapy

Prioritizing intensive treatment of risk factors should be the initial approach to mitigate the risk of cardiovascular and limb events in patients with PAD. Best medical therapy (BMT) comprises weight loss, a balanced diet, quitting smoking, maintaining a regular exercise schedule, and managing CV risk factors. It also includes the best pharmacological therapy (104).

Smoking cessation is the most important modifiable risk factor and is considered a performance measure in the management of patients with PAD. Quitting smoking is associated with improved cardiovascular and limb outcomes. Patients who quit smoking have lower mortality and improved amputation-free survival compared with patients who continue smoking (116).

Exercise therapy is intended to address lifestyle limitations imposed by claudication symptoms of PAD. A meta-analysis of exercise therapy trials found a mean difference of 82.11 m in pain-free walking distance, in addition to improvements in quality-of-life metrics. This study also showed that exercise therapy does not have a clear effect on mortality or amputation rates (117)

Pharmaceuticals used in BMT include lipid-lowering, antithrombotic, and antihypertensive medications. Diabetic individuals are advised to attain optimal control of their glucose levels. A wealth of data indicates statins and other lipid-lowering therapies lower cardiovascular risk in patients with atherosclerotic risk factors (118). Based on the overall beneficial effects of statin, both ACC/AHA and ESC/ESVS guidelines give a class IA indication for statin treatment in all patients with peripheral artery disease. Aspirin or clopidogrel and antihypertensive therapy for all patients with hypertension also have a Level IA to reduce the risk of myocardial infarction, stroke, and vascular death in patients with symptomatic PAD (13).

1.6.2. Endovascular and surgical treatment options

For individuals with severe PAD symptoms like lifestyle-limiting claudication, or non-healing wounds, revascularization presents a viable therapeutic option to prevent the need for amputation. Commonly employed endovascular and surgical interventions comprise bypass grafting, endarterectomy, and angioplasty, with or without stenting (119).

Although in recent decades endovascular devices and techniques have undergone remarkable advancement, conflicting reports from cohort studies on outcomes after endovascular revascularization for PAD have a limited evidence-based approach to PAD management (120, 121). The TASC II Guideline (16) and its supplement published in 2015 (122) both promoted an endovascular-first approach. Global Vascular Guidelines on the management of chronic limb-threatening ischemia (40) introduced new aspects to the appropriate therapeutic approach by showing that bypass surgery using great saphenous vein has similar mortality and amputation outcomes but better expected patency to that of endovascular procedures, although with low-quality evidence. The results of the "Best Endovascular versus Best Surgical Therapy in Patients with CLTI" (BEST-CLI) randomized controlled study also challenge the "endovascular-first" treatment paradigm, showing that the incidence of a major adverse event or death in CLTI was significantly lower after surgical treatment than endovascular therapy, using a single segment of great saphenous vein (96). "Bypass versus Angioplasty in Severe Ischemia of the Leg" (BASIL) 1 study, published over 15 years ago, showed that PVI had a significantly higher early failure rate than bypass surgery (BSX), and clinical outcomes following primary BSX were markedly better than in patients undergoing secondary BSX after PVI. Nevertheless, the recent BASIL-2 results showed better outcomes in the below-the-knee region utilizing endovascular treatment than open surgery (123, 124). The immediate endovascular failure rates have similarly remained stagnant at approximately 15-30% in all trials. Preoperative assessment, risk stratification, and correct indications for endovascular and open surgical procedures are essential for therapeutic decision-making. Still, there is currently no consensus on how to select the right patients that would benefit the most from PVI. With the latest advances in imaging techniques, we can get a more comprehensive and accurate picture of hemodynamic flow, plaque structure, and anatomic complexity to guide optimal treatment planning.

2. Objectives

In recent years, the need for nephroprotective imaging techniques to assist in diagnosing PAD has grown. Since June 2020, QISS MRA has been implemented at the Semmelweis University Heart and Vascular Center, becoming available for the first time in Hungary. Throughout this period, our focus has been on assessing the diagnostic efficacy of this NEMRA protocol in routine patient care:

1. We compared QISS MRA to CO_2 DSA, which is the most commonly used imaging technique in cases of iodinated contrast material sensitivity or impaired renal function.

2. We also compared QISS MRA to DSA using iodinated contrast material, which is still widely used in the diagnosis of PAD.

At the Houston Methodist Hospital, (Houston, Texas, USA), we conducted a proof-of-concept study, where we utilized the above-described AI algorithms:

3. Our study aimed to evaluate the feasibility of employing a custom-made VAE with 2D CNNs to establish a semi-automated classification method of images obtained from PAD lesions, using a specialized, high-resolution 7T MRI histology protocol that incorporates UTE, T1w, and T2w contrasts. This approach may ultimately facilitate the interpretation of MRI images for clinicians, guiding therapeutic decision-making and device selection.

3. Methods

3.1. Comparison of invasive imaging methods and QISS MRA

3.1.1. Study design and patient population

Our research was conducted at the Semmelweis University Heart and Vascular Center between June and December of 2020. Individuals with chronic lower extremity PAD who underwent diagnostic DSA were prospectively enrolled and were scheduled to undergo an additional QISS MRA on the day of their DSA. Inclusion criteria of consecutive patients were as follows: (1) patient presenting symptoms of chronic PAD (>Fontaine IIa); and (2) patient age >18 years. For CO_2 DSA, further inclusion criteria were that (3) GFR was <30; 4) the patient did not consent to the administration of iodinated contrast agent, or 5) there was a documented previous adverse reaction to iodinated contrast media. Patients with (1) an age <18 years; and (2) known contraindications to MRA were excluded. Indication of lower extremity DSA was at the discretion of the primary physician (vascular surgeon or angiologist) and was independent of the current studies. In all cases, the investigators were blinded to the reports and the clinical findings of the patient. All patients provided informed consent. This single-center study was approved by the local and national ethical committees (registration number: OGYEI/7984/2020). All study-related procedures were carried out in accordance with the Declaration of Helsinki.

3.1.2. Imaging protocol

3.1.2.1. DSA using CO_2 and iodinated contrast material

For all patients undergoing diagnostic lower extremity CO_2 DSA, transradial access was employed. Both CO_2 and iodinated contract examinations were conducted by placing 4F pigtail/flush catheters into the terminal aorta. As a standard practice, we performed non-selective contrast injection without table tilting. The decision to use selective injection was at the discretion of the interventional radiologist/vascular surgeon and was only performed when non-selective images were deemed insufficient for treatment planning. An automated injector (Angiodroid, Angiodroid SRL, Bologna, Italy) was used for CO_2 delivery. Images were recorded with a modified CO_2 DSA protocol (Siemens Evenflow, 3–4 frames per second (FPS) of a fixed mount imaging system (Siemens Artis Zee, Siemens Healthineers, Erlangen, Germany) with 60 ml injection volume at 500 mmHg

injection pressure regardless of region. Iodinated contrast material (Ultravist 370, Bayer, Germany) was administered using an automated injector (MEDRAD Avanta, Bayer, Germany).

3.1.2.2. QISS MRA protocol

All QISS MRA scans were conducted using a 1.5T MR scanner (MAGNETOM Aera, Siemens Healthineers, Erlangen, Germany) in feet first, supine patient positioning. A 36-element peripheral angiographic array coil system was utilized in the lower limb region, supplemented with two 18-element torso coils in the abdominal and pelvic regions. QISS MRA scans were acquired in 9-10 steps (depending on patient's height) in transversal plane with fat saturation and venous suppression, starting from the toes and extending to the abdominal aorta. Electrocardiographic (ECG) gating was employed for all measurements in free breathing in the lower extremity and pelvic regions and in breath-hold in the upper abdominal region. Using the acquired transversal plane images, we generated 3D, rotating, coronal plane MIP reconstructions for all patients.

Regarding technical parameters, we used the same settings as Arendt et al. (125) (Table 3).

Table 3.: Technical parameters for Quiescent-Interval Single-Shot Magnetic Resonance Angiography (QISS MRA) examinations as in Arendt et al. (125).

General settings	Orientation: transversal; slices: 50 per one slice group; distance factor: -20%, phase encoding direction: anteroposterior; field of view (FoV) read: 400 mm; FoV phase 65%; slice thickness: 3 mm; voxel size: 0.5x0.5x3.0 mm^3; base resolution 400; phase resolution 100%; phase partial Fourier 5/8
R-R interval <750 ms	Repetition time: 667.62 ms; echo time 1.74 ms; acquisition time 1 min 09 s; flip angle 120°; bandwidth: 658 Hz/Pixel; Generalized Autocalibrating Partial Parallel Acquisition (GRAPPA) with an acceleration factor of 3
R-R interval ≥ 750 ms	Repetition time: 544.40 ms; acquisition time: 6 min 27 s; phase resolution, 100%; acceleration factor of 2

3.1.3. Image analysis

Image processing for CO_2/iodinated contrast material DSA and QISS MRA was conducted on separate workstations: DSA images were processed using Leonardo Workstation (Siemens Healthineers, Erlangen, Germany), while QISS MRA images were evaluated using IMPAX EE workstation (Agfa HealthCare, Bonn, Germany). In both cases, readers aimed to attain the highest image quality by applying optimal post-processing techniques. All CO_2 DSA and QISS MRA images were independently evaluated by two radiologists with ten and four years of expertise in cardiovascular imaging, during individual sessions. Iodinated contrast images were further evaluated by two radiologists, with 5 and 10 years of expertise in PVIs.

Image quality and stenosis grading were assessed for 19 segments as follows: 1—aorta, 2 and 3—bilateral common iliac artery, 4 and 5 —bilateral external iliac artery, 6 and 7—bilateral common femoral artery, 8 and 9—bilateral superficial femoral artery and popliteal artery, 10 and 11—bilateral deep femoral artery, 12 and 13—bilateral tibioperoneal trunk, 14 and 15—bilateral anterior tibial artery, 16 and 17—bilateral posterior tibial artery, 18 and 19—bilateral peroneal artery. Sections that were either not captured in the imaging process or were only partially captured, as confirmed by at least one reviewer, were excluded from the analysis.

Image quality was evaluated using a 5-point Likert scale for each segment: 1—non-diagnostic, image quality inadequate for diagnosis; 2—fair, image quality marginally acceptable for diagnosis; 3—moderate, image quality acceptable for diagnosis; 4—good, image quality adequate for confident diagnosis and 5—excellent, image quality provides a highly confident diagnosis. Prevalence of major artifacts (susceptibility artifact, venous overlay, motion artifact, and arrhythmia-related signal loss) has been listed separately during the assessment of QISS MRA examinations.

Stenoses were categorized using the classification system employed in routine clinical practice, which includes four severity categories: no visible stenosis, degree of stenosis <50%, 50–70%, and >70%. These categories correspond to those utilized in other imaging studies on peripheral artery disease (126, 127). The grading of stenosis primarily relied on visual assessment, and in cases where values were uncertain or borderline, a comparison was made with an intact distal reference parameter. In segments with multiple lesions, the most severe stenosis was recorded.

For statistical analysis, in cases with discrepancies or uncertainties, final values for both image quality and stenosis were determined through consensus reached by the readers. Subsequently, we divided the segments into three distinct anatomical regions (aortoiliac, femoropopliteal, and tibioperoneal) for the final evaluation.

3.1.4. Statistical analysis

Categorical data were presented as frequencies and percentages, while continuous data were expressed as median and interquartile range (IQR). We used Wilcoxon matched-pair test for the comparison of Likert scores. The degree of inter-rater reproducibility was measured by using intra-class correlation coefficient (ICC). Levels of reliability were as follows: poor, ICC < 0.50; moderate, ICC = 0.5–0.74; good, ICC = 0.75–0.90; excellent, ICC > 0.90 (128) given by Koo and Li (2016). Interpretability of both QISS MRA and DSA was assessed by determining the proportion of non-diagnostic segments among all segments, where a Likert score of 2 to 5 was considered as adequate image quality.

The diagnostic accuracy of QISS MRA in detecting obstructive luminal stenosis (>70%) was evaluated on a per-region basis, with CO_2 DSA and iodinated contrast DSA serving as the reference standard. Statistical significance was defined as a two-sided p-value <0.05 for all analyses. All calculations were performed using SPSS statistical software (version 25.0, Armonk, NY, USA).

3.2. Artificial intelligence-aided PAD plaque analysis

This single-center study was carried out in Houston Methodist Hospital, Texas, USA, and was approved by the Institutional Review Board (protocol number: PRO00027258). Informed consent was obtained from all patients, and all procedures were conducted in compliance with the principles outlined in the Declaration of Helsinki.

3.2.1. High-resolution MRI of amputated limbs

Limb specimens from five amputation patients were collected post-surgery. Amputation was indicated in cases of end-stage chronic limb ischemia, a decision independent of the current study. Legs were positioned in an FDA-approved 7T MRI scanner (MAGNETOM Terra, Siemens Healthineers, Erlangen, Germany) with a single-transmit 28-channel knee coil, simulating a clinical setup. The MRI examination, lasting less than one hour, was within the acceptable timeframe for clinical use. The MRI protocol included UTE, T1w

and T2w sequences acquired sagittally with the following parameters: UTE (Pointwise-Encoding Time Reduction with Radial Acquisition (PETRA)): field of view (FOV): 150 mm, phase FOV 100 %, in-plane resolution 0.2x0.2 mm, slice thickness: 0.2 mm, TR 10 ms, TE 0.07 ms, flip angle (FA) 4; T2w (Double Echo Steady State (DESS): FOV 160 mm, phase FOV 87.5 %, slice thickness 0.2 mm, TR 12.57 ms, TE 6 ms, FA 25, water excitation, 512 slices). T1w (3D Fast Low-Angle Shot (FLASH): FOV 160 mm, phase FOV 87.6 %, in-plane resolution 0.2x0.2 mm, slice thickness 0.2 mm, TR 9.5 ms, TE 4.09 ms, FA 7, Generalized Auto-Calibrating Partially Parallel Acquisitions (GRAPPA) 2, phase encode direction A>>P, 512 slices, water excitation).

3.2.2. Image preprocessing

Datasets containing T1w, T2w and UTE image contrasts were co-registered using the General Registration module in 3D Slicer software (129). The co-registration process utilized the options 'useMomentsAlign' and 'Rigid+Scale, 7 degrees of freedom'. The aligned volumes were then exported in Neuroimaging Informatics Technology Initiative (NIFTI) format and imported into ImageJ software (114). To equalize image contrasts, the images were normalized across all lesions. The normalized images for the three contrasts (T1w, T2w, and UTE) were combined to create pseudo red-green-blue (RGB) images. The T1w images were assigned as the red component, the T2w images as the green component, and the UTE images as the blue component. Each PAD lesion was manually outlined in the acquired sagittal orientation. The outlined volumes were then resliced with the original resolution to generate axial MPR reconstructions. Each axial slice was further outlined utilizing the ‘Auto-Crop’ function available in ImageJ and resized to 64x64 pixels. To extract hard/soft components (i.e. dark blue/black and blue, respectively), pixels with hexadecimal RGB values ranging from 0x800000 to 0xff0000 were removed.

3.2.3. Variational autoencoder

Two 2D convolutional neural networks were developed, with the pre-processed images serving as input for the first network. Starting with a 2D input layer comprising three channels for the pseudo-color RGB images, we constructed five convolutional layers with increasing depth (Figure 9B). The final layer, the output layer, was flat fully connected with the same number of elements as the last convolutional layer. This output layer was

fed into two separate layers: the mean layer and the variance layer. Both layers were of the same dimension (2D) as the latent space and represented the mean and variance for two Gaussian distributions. Using these mean and variance values, the representation of each image was calculated based on its coordinates (x and y components) in latent space (Figure 9B). The VAE model was implemented on a MacBook Pro (Apple Inc., Cupertino, CA, USA) equipped with the M1 chip, utilizing TensorFlow (version 2.7.0, Google, Mountain View, CA, USA) in Python (version 3.9.9, Python Software Foundation, Austin, TX, USA) with a virtual environment created with Conda (version 4.11.0, Anaconda Inc., Austin, TX, USA). The TensorFlow-Metal Pluggable Device (version 0.8.0, Mountain View, CA, USA) was implemented to allow the use of the Apple M1 Graphics Processing Unit (GPU) approximately accelerate computations by an order of magnitude. With a total of 500 epochs, batch size of 128 and a learning rate of 0.0005 (Adam optimizer), the VAE was trained.

3.2.4. Tissue Classes and latent space classification

By analyzing the reconstructed axial luminal cross-sections (hard/soft tissue as black/blue) in the latent space, we visually divided it into four regions, each representing a tissue class associated with PAD. Each tissue class was assigned a numerical tissue score as follows: Tissue Class 1: lumen patent, tissue score 0; Tissue Class 2: lumen partially patent, tissue score 1; Tissue Class 3: lumen mostly occluded with soft tissue, tissue score 3 and Tissue Class 4: lumen mostly occluded with hard tissue, tissue score 5 (Figure 9A). To determine the overall tissue characteristics of each lesion sample, an average tissue score was calculated by averaging the tissue scores assigned to each cross-section within the lesion. Relative percentages of each tissue class were determined to provide further insights into the lesion’s composition.

DOI:10.14753/SE.2024.3024

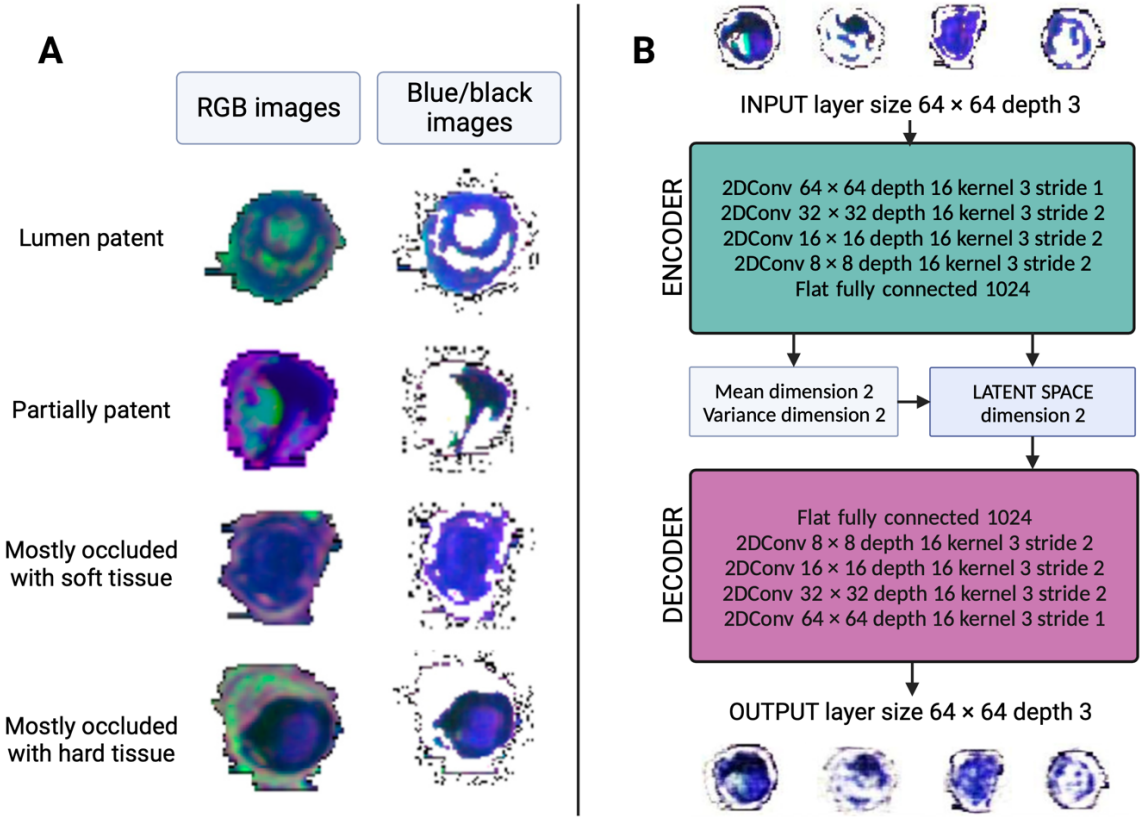

Figure 9: (A) Representative cross-sections of pseudo-color red-green-blue (RGB) images, (T1-weighted in red), T2-weighted in green, and Ultrashort Echo Time in blue), along with corresponding blue/black images for the four tissue classes. (B) Schematic illustration of the variational autoencoder (VAE), providing specific parameters for both the encoder and decoder layers. At the top, representative input cross-sections, while at the bottom, corresponding cross-sections reconstructed by the VAE are displayed. In this setup, the VAE takes pseudo-color images as input. The encoder component utilizes multiple neural network layers with varying resolutions, kernel sizes, and strides to compress the input into the latent space. The encoder reduces the dimensionality of the data while extracting relevant features. The decoder takes the information sampled from the latent space as input and aims to reconstruct output cross-sections that closely resemble the input in a series of steps, mirroring the encoder but in reverse order. (2DConv - Two-Dimensional Convolutional Layer; 2DConvTrans - Two-Dimensional Transposed Convolutional Layer)

4. Results

4.1. Comparison of invasive imaging methods and QISS MRA

4.1.1. Comparison of CO_2 DSA and QISS MRA

A total of 28 patients (11 male, mean age 71 ± 9 years) were included in our study. Detailed patient characteristics are presented in Table 4. Eight QISS MRA segments (four aortas, four common iliac arteries) and one CO_2 DSA segment (anterior tibial artery) were excluded due to partial imaging, leaving 523 segments for final evaluation. These segments were examined across 164 prioritized regions (aortoiliac, femoropopliteal, and tibioperoneal).

Table 4.: Characteristics of the patient population for the comparison of carbon dioxide digital subtraction angiography and Quiescent-Interval Single-Shot Magnetic Resonance Angiography. (BMI: body mass index; eGFR: estimated glomerular filtration rate; KDOQI: Kidney Disease Outcomes Quality Initiative)

Parameters	**Patients (n=28)**
General parameters	
Age (years)	71 [68-77]
Female sex , N (%)	17 (60.7)
Height (cm)	167 [158-172]
Weight (kg)	79 [67-86]
Atherosclerotic risk factors	
BMI >25 kg/m^2, N (%)	21 (75.0)
Smoking (current and former), N (%)	25 (89.3)
Hypertension, N (%)	17 (60.7)
Dyslipidemia, N (%)	7 (25.0)
Diabetes mellitus, N (%)	10 (35.7)
Chronic renal insufficiency	
eGFR (ml/min/1.73 m2)	55 [35-72]
KDOQI stage II, N (%)	11 (39.3)
KDOQI stage III, N (%)	10 (35.7)
KDOQI stage IV, N (%)	6 (21.4)
Peripheral arterial disease	
Fontaine stage IIa, N (%)	2 (7.2)
Fontaine stage IIb, N (%)	14 (50.0)
Fontaine stage III, N (%)	2 (7.1)
Fontaine stage IV, N (%)	8 (28.6)
Other comorbidities	
Coronary artery disease, N (%)	2 (7.1)
Arrythmia, N (%)	6 (21.4)

4.1.1.1. Image quality

QISS MRA outperformed CO_2 DSA in terms of image quality across all regions. QISS MRA consistently demonstrated a median of good image quality in all cases. The majority of CO_2 angiographies exhibited only a median of moderate image quality, with the femoropopliteal region presenting a median of good image quality (QISS MRA vs. CO_2 DSA; all regions: 4 [4-5] vs. 3 [3-4]; aortoiliac region: 4 [4-5] vs. 3 [3-4]; femoropopliteal region: 4 [4-5] vs. 4 [3-4]; tibioperoneal region: 4 [4-5] vs. 3 [2-3]; all $p<0.001$) (Figure 10).

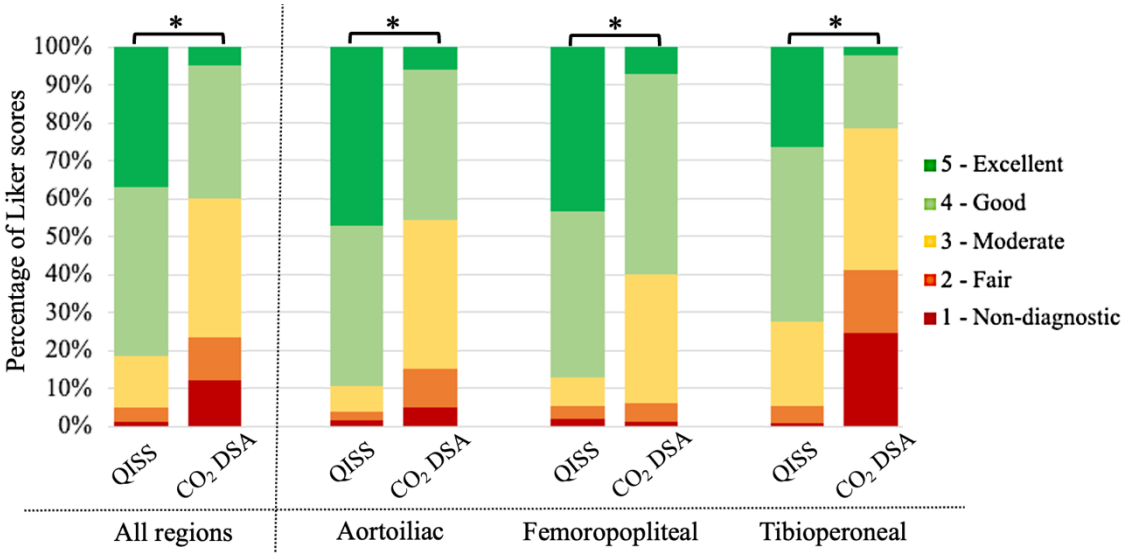

Figure 10: Per-region comparison of Likert scores in subjective image quality assessment of QISS MRA and CO_2 DSA datasets. (DSA: digital subtraction angiography, QISS MRA: Quiescent-Interval Single-Shot Magnetic Resonance Angiography)

4.1.1.2. Diagnostic accuracy

Diagnostic accuracy parameters of QISS MRA were assessed for significant (>70%) stenosis using sensitivity, specificity, positive predictive value (PPV), negative predictive value (NPV), and diagnostic accuracy, with CO_2 DSA serving as the reference standard. The results are as follows: sensitivity 82.6% [95% CI, 74.1-89.2%], specificity 96.9% [95% CI, 94.6-98.5%], PPV 89.1% [95% CI, 82.0-93.6%], NPV 94.8% [95% CI, 91.0-95.6%], and diagnostic accuracy 93.6% [95% CI, 91.0-95.6%].

4.1.1.3. Interpretability

A comparison of the percentage of segments providing adequate diagnostic image quality showed that for all regions combined, interpretability is superior with QISS MRA compared to CO_2 DSA (98.3% vs 86.2%; p<0.001). In the tibioperoneal region, the difference between the two modalities was even more pronounced: 99.1% of QISS MRA images had an image quality adequate for diagnosis, whereas for CO_2 DSA this value was only 71.7% (n/N=221/223vs. n/N=160/223, respectively; p<0.001).

Table 5.: Per-region comparison of interpretability between CO_2 DSA and QISS MRA. (CO_2 DSA: carbon dioxide digital subtraction angiography, QISS MRA: Quiescent-Interval Single-Shot Magnetic Resonance Angiography)

	QISS MRA	**CO_2 DSA**	**p-value**
All regions, % (n/N)	98.3 (514/523)	86.2 (451/523)	***<0.001***
Aortoiliac region, % (n/N)	96.7 (128/132)	94.7 (125/132)	0.36
Femoropopliteal region, % (n/N)	98.2 (165/168)	98.8 (166/168)	0.67
Tibioperoneal region, % (n/N)	99.1 (221/223)	71.7 (160/223)	***<0.001***

4.1.1.4. Reproducibility

QISS MRA also demonstrated superior performance in the classification of stenoses: inter-observer agreement showed better reproducibility for QISS MRA than CO_2 DSA in all examined regions. Interobserver ICC for QISS MRA was 0.97 for all regions, 0.95 for the aortoiliac region, 0.97 for femoropopliteal region, 0.97 for tibioperoneal region. In contrast, ICC values for CO_2 DSA were 0.81, 0.80, 0.85 and 0.78 for the corresponding regions, respectively (Table 6).

Table 6: Per-region assessment of interobserver reproducibility for stenosis grading using intraclass correlation coefficient comparing CO_2 DSA to QISS MRA. (CO_2 DSA: carbon dioxide digital subtraction angiography. All p<0.001. QISS MRA: Quiescent-Interval Single-Shot Magnetic Resonance Angiography, CI: confidence interval)

	QISS MRA	**CO_2 DSA**
All regions	0.97 [95% CI, 0.96–0.97]	0.81 [95% CI, 0.73–0.86]
Aortoiliac region	0.95 [95% CI, 0.93–0.96]	0.80 [95% CI, 0.63–0.90]
Femoropopliteal region	0.97 [95% CI, 0.96–0.80]	0.85 [95% CI, 0.75–0.91]
Tibioperoneal region	0.97 [95% CI, 0.96–0.98]	0.78 [95% CI, 0.67–0.87]

4.1.2. Comparison of iodinated contrast material DSA and QISS MRA

After excluding 23 segments due to partial imaging, we evaluated a total of 623 segments from 34 patients (24 men, mean age 67±5 years). Detailed characteristics of the patient population are shown in Table 7.

Table 7: Characteristics of the patient population for the comparison of iodinated contrast digital subtraction angiography and Quiescent-Interval Single-Shot Magnetic Resonance Angiography. Continuous variables are described as median and interquartile range, whereas categorical variables are represented as frequencies and percentages. (BMI: body mass index; eGFR: estimated glomerular filtration rate; KDOQI: Kidney Disease Outcomes Quality Initiative)

Parameters	Patients (n=34)
General parameters	
Age (years)	67 [62-72]
Female sex, N (%)	10 (29.4)
Height (cm)	170 [162-174]
Weight (kg)	74 [66-90]
Atherosclerotic risk factors	
BMI >25 kg/m^2, N (%)	19 (55.8)
Smoking (current and former), N (%)	24 (70.6)
Hypertension, N (%)	24 (70.6)
Dyslipidemia, N (%)	16 (47.1)
Diabetes mellitus, N (%)	22 (64.7)
Chronic renal insufficiency	
eGFR (ml/min/1.73 m2)	81 [62-90]
KDOQI stage II, N (%)	19 (55.9)
KDOQI stage III, N (%)	5 (14.7)
KDOQI stage IV, N (%)	1 (2.9)
Peripheral arterial disease	
Fontaine stage IIa, N (%)	2 (5.9)
Fontaine stage IIb, N (%)	12 (35.3)
Fontaine stage III, N (%)	5 (14.7)
Fontaine stage IV, N (%)	1 (2.9)
Other comorbidities	
Coronary artery disease, N (%)	9 (26.5)
Stroke, N (%)	4 (11.8)

4.1.2.1. Image quality

Following consensus assessment, our results indicated that QISS MRA yielded significantly better subjective image quality than DSA for all regions combined and for the below-the-knee region (QISS vs. DSA; all regions: 4 [4-5] vs. 4 [3-5]; tibioperoneal region: 4 [4-5] vs. 3.5 [3-4], both p<0.001). In the aortoiliac and femoropopliteal regions, QISS MRA provided a median of good image quality, comparable to DSA, however, DSA outperformed QISS MRA (aortoiliac region: 4 [4-4] vs. 4 [4-5], p<0.001; femoropopliteal region: 4 [4-4] vs. 4 [4-5], respectively, p=0.01) (Figure 11).

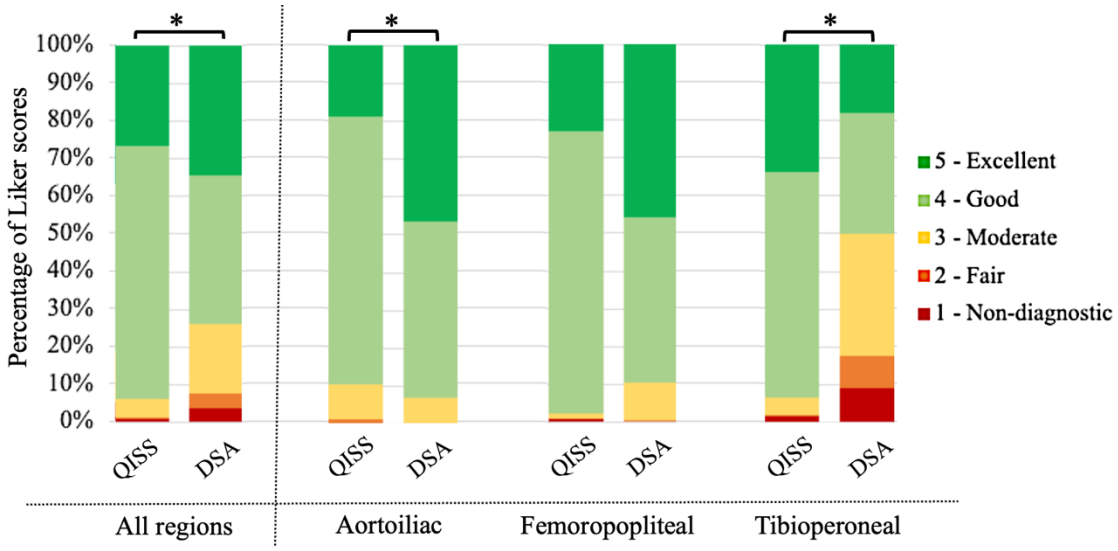

Figure 11: Per-region comparison of Likert scores in subjective image quality assessment of QISS MRA and iodinated contrast DSA images. (DSA: digital subtraction angiography, QISS MRA: Quiescent-Interval Single-Shot Magnetic Resonance Angiography)

4.1.2.2. Diagnostic accuracy

Diagnostic accuracy of QISS MRA in detecting significant (>70%) stenosis was evaluated using iodinated contrast DSA as the reference standard, yielding a sensitivity of 84.8% [95% CI, 77.3-90.6], specificity of 93.0% [95% CI, 90.3-95.1], PPV of 76.3% [95% CI, 69.6-81.8], NPV of 95.8%, and diagnostic accuracy of 91.3% [95% CI, 88.7-93.4].

4.1.2.3. Interpretability

Significant interpretability differences were observed between the two modalities across all regions. QISS MRA displayed superior image quality, with only 1% of segments (6/623) deemed non-diagnostic, compared to 3.9% (24/623) with DSA (p<0.001). Particularly in the below-the-knee area, QISS MRA performed even better, with only 0.6% (4/623) segments showing unsatisfactory image quality, while DSA had 9.1% (24/623) non-diagnostic segments, six times higher than QISS MRA (p<0.001) (Table 8).

Table 8.: Per-region comparison of interpretability between iodinated contrast DSA and QISS MRA. DSA: carbon dioxide subtraction angiography, QISS MRA: Quiescent-Interval Single-Shot Magnetic Resonance Angiography)

	QISS MRA	DSA	p-value
All regions (%, n/N)	99 (617/623)	96.1 (599/623)	<0.001
Aortoiliac region (%, n/N)	100 (160/160)	100.0 (160/160)	1.00
Femoropopliteal region (%, n/N)	99 (197/199)	100.0 (199/199)	0.32
Tibioperoneal region (%, n/N)	98.5 (260/264)	90.9 (240/264)	<0.001

4.1.2.4. Reproducibility

For stenosis assessment, inter-rater ICC for Likert scores was 0.94 [95% CI, 0.93-0.95] for QISS MRA, indicating excellent agreement between observers. Conversely, for DSA, the ICC was lower at 0.88 [95% CI, 0.86-0.90], suggesting higher variability in ratings (Table 9).

Table 9: Per-region assessment of reproducibility for stenosis grading using intraclass correlation coefficient (ICC), comparing iodinated contrast DSA to QISS MRA. All p<0.001. (DSA: digital subtraction angiography; QISS MRA: Quiescent-Interval Single-Shot Magnetic Resonance Angiography, CI: confidence interval)

	QISS MRA	DSA
All regions	0.94 [95% CI, 0.93-0.95]	0.88 [95% CI, 0.86-0.90]
Aortoiliac region	0.91 [95% CI, 0.87-0.93]	0.79 [95% CI, 0.71-0.84]
Femoropopliteal region	0.92 [95% CI, 0.89-0.94]	0.90 [95% CI, 0.87-0.93]
Tibioperoneal region	0.95 [95% CI, 0.94-0.97]	0.86 [95% CI, 0.81-0.89]

4.2. Artificial intelligence-aided PAD plaque analysis

4.2.1. Image preprocessing

A total of 2390 MPR images were obtained from the original five lesion samples, with the distribution as follows: Sample #1: 168 images, Sample #2: 453 images, Sample #3: 943 images, Sample #4: 514 images, and Sample #5: 312 images. To enhance visual representation, pseudo-colors were assigned to different components based on the MRI contrasts used. The arterial wall was represented by red/pink, the free lumen/blood by green, calcium by black, collagen by dark blue, and soft tissue by bright blue (Figure 9A) colors. By removing the RGB pixels as described in the Methods section, the remaining pixels represented the hard and soft tissues, appearing as black and blue, respectively (Figure 9A and Figure 12).

4.2.2. Variational Autoencoder

Upon visual inspection, the comparison between the original images and the AI-reconstructed pseudo-color images revealed a high level of agreement, indicating successful implementation of the trained 2D CNN VAE. The colors and their spatial distribution in the reconstructed images closely matched those of the original images, with only slight blurring observed in the reconstructed axial slices (Figure 9B). Based on the distribution of the reconstructed axial slices in the latent space, the space was divided into four distinct regions, each corresponding to a specific tissue class. The boundaries for these regions were determined by assigning values to the x and y-components in the latent space as follows: Tissue Class 1: lumen patent, x-value < 0.8, y-value < .8; Tissue Class 2: lumen partially patent; x-value < 0.8, y-value > 0.8; Tissue Class 3: lumen mostly occluded with soft tissue, x-value > 0.8, y-value ≤ 0.8 and Tissue Class 4: lumen mostly occluded with hard tissue, x-value > 0.8 and y-value ≤ 0.8 (Figure 12).

DOI:10.14753/SE.2024.3024

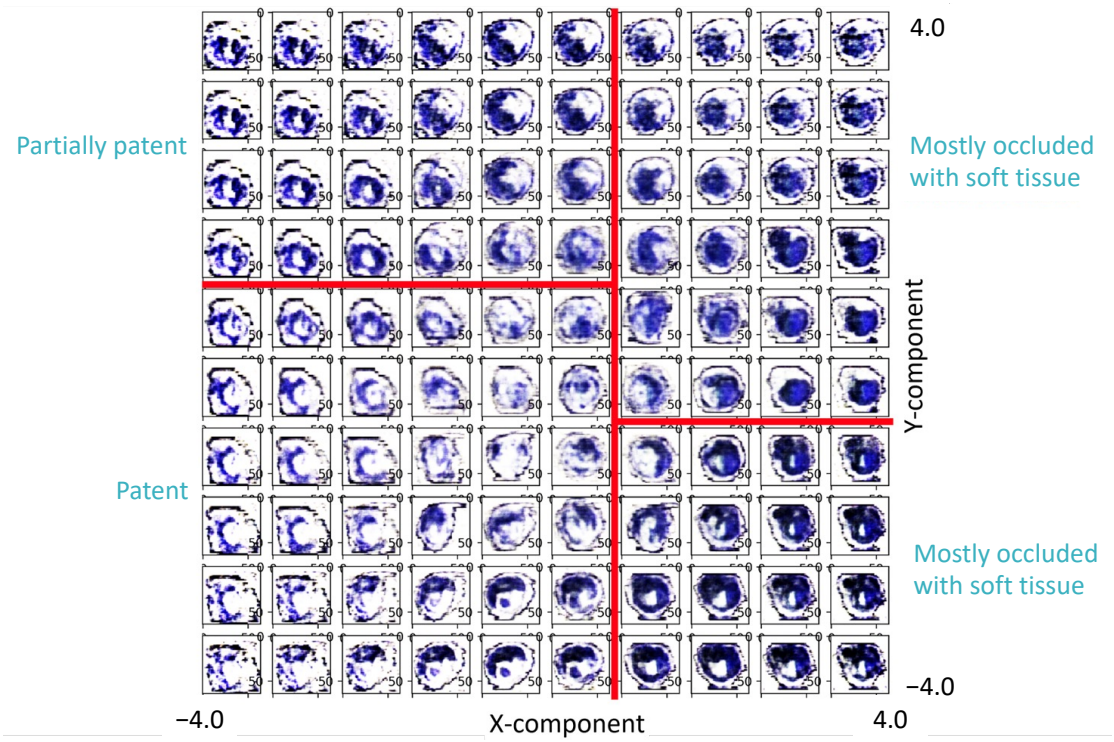

Figure 12: Distribution of the reconstructed cross-sections in the latent space is visualized based on the x and y-components. Boundaries are delineated in red to separate the latent space into subregions, representing the four tissue classes associated with peripheral artery disease (PAD) lesions. Soft PAD lesion components appear as blue, hard components are represented in black, while patent lumen appears as white.

4.2.3. Tissue scores

Distribution of the tissue scores for the axial slices closely aligned with the visual inspection of each tissue. Tissue scores varied in range: in lesion sample #1, only Tissue Class 1 was present, indicating a completely patent lumen, with an average tissue score of 0. Lesion sample #3 (average tissue score: 1.06) predominantly featured partially patent regions (Tissue Class 2), with two focal areas showing mostly occluded lumens with soft tissue (Tissue Class 3). Lesion samples #2 (average tissue score 1.33) and #5 (average tissue score 1.44) exhibited similar patterns, with larger regions corresponding to Tissue Class 2 than Tissue Class 3. In lesion sample #4, a significant portion of Tissue Class 4 was surrounded by adjacent Tissue Class 3 regions, resulting in the highest average tissue score observed (2.47). The relative percentages of Tissue Classes for lesion samples #2-#5 demonstrated that Tissue Class 2 had the highest representation, followed by Tissue Class 3 and Tissue Class 1. (Table 10 and Figure 13).

DOI:10.14753/SE.2024.3024

Table 10: Relative percentages of Tissue Classes for each lesion sample (#1-#5).

Sample number	Tissue Class I (%)	Tissue Class II (%)	Tissue Class III (%)	Tissue Class IV (%)
#1	100	0	0	0
#2	4.2	75.9	19.9	0
#3	9.8	72.2	18	0
#4	0.2	46.3	33.5	20
#5	5.8	69.6	24.7	0

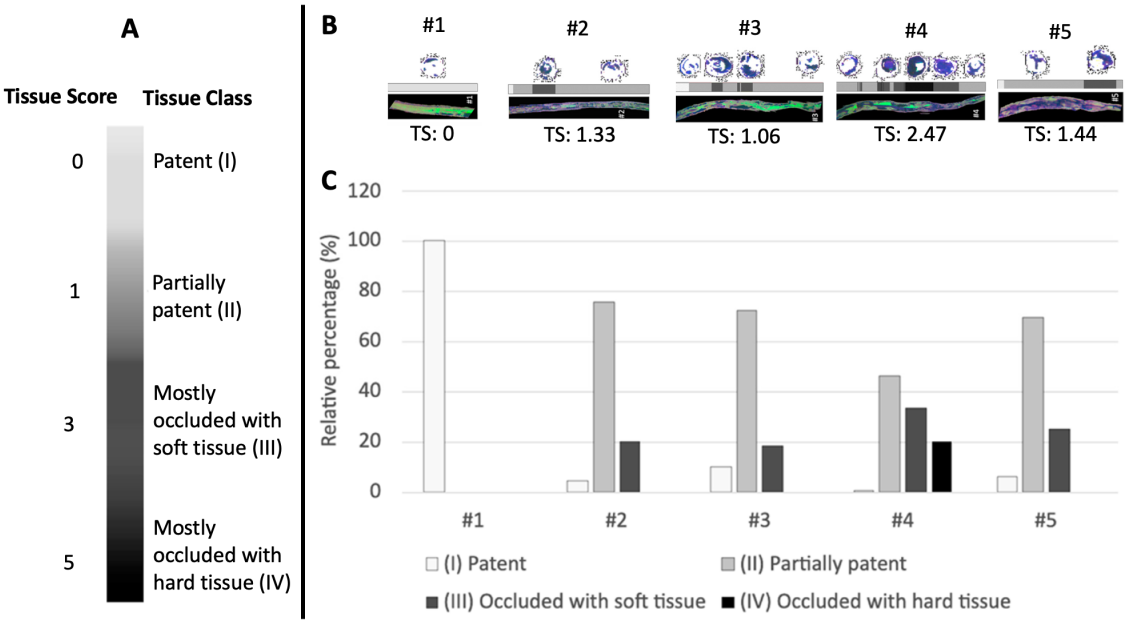

Figure 13: A) Grayscale-coded display of determined Tissue Classes based on tissue scores for each slice, used for (B,C). (B) Centerline pseudo-color red-green-blue images (T1-weighted—red, T2-weighted—green, Ultrashort Echo Time—blue) are displayed for each of the five lesions (numbered #1–#5). Above, greyscale-coded display of the determined Tissue Classes across the lesion and representative VAE output images. Average tissue scores for all lesions are given below. (C) Percentage distribution of tissue scores for each lesion (#1–#5) in greyscale color as per subfigure "A". (PAD: Peripheral Artery Disease. TS: Tissue Score. VAE: variational autoencoder)

5. Discussion

5.1. QISS MRA in the diagnosis of peripheral arterial disease

Our research focused on evaluating recent advancements in MRI for diagnosing PAD. In our first study, we compared QISS MRA with CO_2 DSA, which is commonly used as the preferred diagnostic method in patients with iodinated contrast material sensitivity and impaired renal function. Next, we compared QISS MRA with iodinated contrast material DSA, the current gold standard for diagnosing PAD, particularly in below-the-knee arteries.

QISS MRA outperformed CO_2 DSA regarding image quality and exhibited superior interpretability across all examined regions. Notably, our study highlighted a substantial difference in image quality between the imaging modalities for the below-the-knee region. The number of non-diagnostic segments, in general, was negligible for QISS MRA, exhibiting the most pronounced difference in the tibioperoneal region. The ICC demonstrated excellent reproducibility of QISS MRA across all examined regions for the assessment of stenoses. In contrast, CO_2 DSA showed reliable reproducibility solely in the aortoiliac region, with the most significant disparity between the methods once more observed in the tibioperoneal region. The smallest difference in image quality was observed in the femoropopliteal region, where both techniques produced images of good quality.

Compared to iodinated contrast DSA, QISS MRA had better image quality in all regions combined, and this difference was again even more pronounced in the tibioperoneal region. Although iodinated DSA generally exhibited superior image quality in the aortoiliac and femoropopliteal regions, which aligns well with the experience in routine clinical practice, QISS MRA still provided at least good image quality in these vascular segments. QISS MRA also demonstrated superior interpretability in all regions, especially in the tibioperoneal region. Additionally, QISS MRA showed excellent ICC scores for stenosis assessment across all regions, whereas DSA only demonstrated excellent reproducibility for the femoropopliteal region. These results suggest that QISS MRA is a reliable tool for evaluating lower extremity arterial stenosis, even when compared to the established “gold standard” iodinated DSA.

In everyday clinical practice, a thorough knowledge of the disadvantages and advantages of different imaging techniques in the diagnosis of PAD is of paramount importance. The

advantages and disadvantages of QISS MRA, CO_2 DSA and iodinated contrast DSA are summarized in Table 11. Clinicians generally determine the optimal imaging modality for the patient considering the symptoms, medical history of the individual, and the potential risks of the imaging modalities. In comparison to CTA and DSA, MRI remains an underrecognized method in diagnosing PAD; however, it shows immense promise in addressing critical knowledge gaps for effective treatment planning. The current AHA/ACC (13) and ESC/ESVS Guidelines (2) position DUS, CTA, MRA, and DSA at a similar level in treatment planning, lacking differentiation in their optimal usage for specific purposes. Both the Global Vascular Guidelines of the Society for Vascular Surgery (40) and the NICE (130) guidelines for CLTI underscore the urgency of advancing non-invasive PAD imaging, particularly using MRI. DSA, being an invasive procedure, carries certain risks. The procedure may cause blood clot formation at the puncture site or within the blood vessels being examined. Arterial wall damage related to the examination process may also result in pseudoaneurysms or hematoma formation and less commonly, dissection at the puncture site (131). Before undergoing invasive procedures, comprehensive monitoring of coagulation parameters is essential. These procedures typically entail patients spending several hours in healthcare facilities, with potential complications necessitating several days of care. While the complication rate is typically less than 1% (132), financial considerations, as well as the psychological and physical burden on patients, may make it more favorable to prioritize the use of non-invasive diagnostic alternatives. Thus, QISS MRA, being completely non-invasive, can often be a superior choice for PAD diagnosis.

Regarding diagnostic performance parameters, QISS MRA demonstrated reliable accuracy, exhibiting exceptionally high specificity (96.9% and 93.0%), NPV (94.8% and 95.8%), and diagnostic accuracy (93.6% and 91.3%) compared to CO_2 DSA and iodinated contrast DSA. Similar values were reported in a previous study by Arendt et al. (sensitivity 91.5%, specificity 94.2%, NPV 96.6%) on a smaller patient population (125) compared to CO_2 DSA, as well as in other studies (Hodnett et al. 87-92% sensitivity, 96-97% specificity (133); Altaha et al. 92% and 95%, respectively (134)) using DSA as a standard of reference. The only existing meta-analysis on the diagnostic performance of QISS MRA showed a pooled 88% sensitivity and 94% specificity on a per-segment basis with DSA or contrast-enhanced MRA as reference standard.

Challenges in diagnosing cases with reduced renal function or contrast sensitivity should also be highlighted. The 2018 update of the 2012 National Institute for Health and Care Excellence (NICE) guideline emphasized the need for research on the clinical and cost-effectiveness of diagnostic tools for PAD in patients with diabetes (130). The use of iodinated contrast media in DSA studies significantly increases the risk of contrast-induced nephropathy. As an alternative, carbon dioxide gas is used in everyday clinical practice to replace nephrotoxic iodinated contrast agents. However, the resulting image quality is inferior to that of conventional iodinated contrast media (62). Over the last decade, there has been a significant reduction in the incidence of NSF associated with MRI contrast media admission (135). Yet, current data regarding the retention and buildup of gadolinium in the body has reignited safety concerns surrounding gadolinium-based contrast agents (GBCAs). This decline in NSF cases can be attributed to several factors, including improved screening of renal function in patients who receive GBCAs, development and utilization of more thermodynamically stable GBCAs, and the proper administration of GBCAs in individuals undergoing MRI scans with contrast enhancement. The most recent 2020 American College of Radiology Guidelines (136) and 2018 European Society of Urogenital Radiology Guidelines (137) still identified those with eGFR <30mL/min/1.73 m^2 without dialysis at risk of developing NSF. Compared to DSA and CEMRA techniques, non-contrast methods like QISS MRA offer the advantage of not requiring pre-screening for renal function and eliminating the risk of side effects associated with contrast agents. However, limited international literature data exist comparing the diagnostic performance of QISS MRA and other nephroprotective techniques. To date, only one retrospective study has compared CO_2 DSA and QISS MRA. (125). This study, conducted by Arendt et al., included a small cohort of 16 chronic PAD patients who underwent both CO_2 DSA and QISS MRA within a 90-day period. Arendt et al. demonstrated the superior diagnostic performance of the QISS protocol over CO_2 DSA. They also reported that QISS MRA provided better subjective image quality compared to invasive CO_2 angiography in all regions examined. The authors attributed the high interpretability of QISS MRA to its low incidence of artifacts. Our study findings are consistent with their published data, affirming that QISS MRA is a promising and safer option for individuals with impaired renal function compared to CO_2 DSA.

Among nephroprotective techniques, NEMRA sequences are another option to consider. QISS MRA has demonstrated better performance and greater or comparable reliability when compared to alternative NEMRA sequences. In comparison to 3D turbo spin-echo (TSE)-based subtraction MRA, QISS MRA received good to excellent ratings in 79.5% to 96.0% of segments, with no segments rated as non-diagnostic, while for 3D TSE-based subtraction MRA, 89.8% to 96.1% of segments had non-diagnostic or poor image quality (134). Of note, in our patient population, 1.72% and 1% of segments were non-diagnostic for QISS MRA. In comparison to flow-sensitive dephasing (FSD), both FSD and QISS achieved similar high sensitivity and negative predictive value in detecting over 50% stenosis. FSD exhibited slightly superior diagnostic specificity and offered better visualization of arterial lesions due to its submillimeter spatial resolution. However, as a more user-friendly and time-efficient technique, QISS could be the method of preference for rapid scanning of lower extremity PAD (138). In comparison to Native SPACE NEMRA technique, QISS MRA exhibited higher specificity and image quality, and demonstrated increased robustness in the abdominal and pelvic regions (89).

Reduced flow parameters in DSA can compromise image quality, making accurate diagnoses and treatment planning challenging. In patients with PAD, contrast material may not reach the distal lower limb due to reduced hemodynamic properties and multilevel stenoses. Selective contrast material administration during DSA scans can help maintain adequate image quality when evaluating specific distal arterial segments. Nevertheless, this technique extends procedure duration and increases radiation dose. Our findings indicate that QISS MRA provides superior image quality in the tibioperoneal region, commonly affected by reduced blood flow, without ionizing radiation or contrast agents (Figures 14 and 15). Offerman et al. had similar findings when comparing the flow dependency of TOF, ECG-gated 3D FSE, and ungated 3D FSE ghost MRA to QISS MRA. The latter demonstrated the most robust accuracy in depicting normal lumen and stenosis under a wide range of flow conditions (139). Even in cases with normal renal function parameters, if severe vascular stenosis in the below-the-knee region is suspected based on initial physical assessment, the use of QISS MRA should be considered due to its high diagnostic performance.

One additional key advantage of QISS MRA over DSA is its ability to acquire three-dimensional data, enabling multi-orientational image analysis. Rotating coronal MIP

reconstructions or CMPRs can easily be generated from QISS MRA data. DSA images are obtained via summation X-ray techniques, usually depicting only the antero-posterior image plane (or other planes if the table or C-arm is tilted). Repeated radiation exposure and contrast media administration are required if a different image plane is needed for diagnosis. Hence, QISS MRA offers greater post-processing flexibility than DSA.

One potential limitation of QISS MRA is its inability to fully map the abdominal aorta in particularly tall patients using the standard setup. In such cases, missing segments can be captured separately in an additional measurement specifically adjusted for that region. Additionally, the relatively long scan time (20-30 minutes) of QISS MRA poses a challenge as motion artifacts, mimicking stenosis, can limit the assessment of QISS MRA images. To ensure optimal image quality and minimize motion artifacts, patients must remain completely still throughout the image acquisition process. However, this can be problematic for patients with PAD experiencing rest pain, as maintaining a fixed posture without movement for a longer period may be difficult. Notably, motion artifacts are also common in DSA studies but can be reduced through image post-processing. Literature data suggests that respiratory artifacts can also limit the image quality of QISS MRA images in the abdominal and pelvic regions (94). To address this issue, we acquired images in these regions during breath-hold, and in our study population, we found that respiratory artifacts did not significantly impair the image quality of QISS MRA.

QISS MRA, being an ECG-gated imaging technique, may encounter artifacts with irregular heart rates. In our study, despite observing satisfactory image quality even in patients with irregular heart rates, scan duration was prolonged due to challenges in obtaining accurate readouts. To address this issue, Edelman et al. developed an ungated variant called “Ungated Quiescent-Inflow Single-Shot” (UnQISS) sequence, with a scan time of 15.4 minutes (140). However, limited data exists on UnQISS, with no studies conducted thus far to compare its performance with ECG-gated QISS MRA.

The image quality of QISS MRA, like other MRI techniques, can be affected by susceptibility artifacts from metallic implants. While certain implants, such as MRI conditional hip and knee replacements, are not contraindications for MRI scans, they can make assessing vascular status challenging. Moreover, there is a lack of precise data on visualizing stents (such as cobalt-chromium balloon-expandable or nitinol self-expandable stents) previously implanted in the iliac or femoropopliteal system. In our

study, we encountered a patient with a stent implanted in the external iliac artery (Omnilink Elite, Abbott Laboratories, Abbott Park, Illinois). We observed that this particular stent did not significantly affect the image quality of the QISS MRA. Although the findings of Varga-Szemes et al. suggest that the varied imaging appearance of stents and severity of artifacts in QISS MRA studies (ranging from no signal to excellent visibility) can be attributed to the different stent architectures (125), there is currently no comprehensive study available in the international literature addressing this specific issue.

QISS MRA, similarly to other bright blood NMRA sequences with tissue saturation is only capable of visualizing the vessel lumen and is unable to accurately depict the vessel wall. However, combining novel proton density-weighted, gradient echo sequences (141) or UTE imaging (70) with QISS MRA allows us to get detailed knowledge of complex plaque characteristics, thus further guiding PAD treatment planning.

One disadvantage of CO_2 DSA is the presence of artifacts caused by intestinal gases, which can significantly limit the accurate visualization of abdominal and pelvic regions (Figure 16). Conversely, QISS MRA scans are unaffected by artifacts caused by intestinal gases. Furthermore, CO_2 contrast material often breaks down into small bubbles, leading to partial filling of wider-diameter blood vessels. This fragmentation of the contrast bolus can produce a "cobblestone-like" appearance, resembling "pseudostenosis" in lower extremity arteries. To ensure consistent filling of vessels, CO_2 angiography requires higher frame rates per second for satisfactory image quality, resulting in elevated radiation exposure. The implementation of newly developed computerized CO_2 injectors and advanced image processing techniques, like DVA, can enhance image quality when using CO_2 contrast material. CO_2 administration may also cause non-serious adverse effects, discomfort, and movement during the procedure, resulting in artifacts and reduced image quality. In contrast, QISS MRA, being a contrast and radiation-free examination, is painless for patients, except for potential discomfort associated with the supine, dependent position. Additionally, QISS MRA is free from bone or calcified plaque interference observed in DSA images.

It is also important to note that the image quality of both modalities is highly dependent on the technical aspects of the MRI scanner or fluoroscopic equipment, including factors such as the manufacturer, model, magnetic field strength, and homogeneity. The

individual anatomy of the patient and, in the case of DSA, the expertise of the interventional radiologist or vascular surgeon can also impact image quality.

In summary, QISS MRA demonstrates excellent diagnostic accuracy, being superior to CO_2 DSA and comparable to iodinated contrast DSA. The most significant difference observed in our studies between QISS MRA and DSA was in the tibioperoneal region. DSA image quality can be compromised by factors like reduced blood flow velocity and patient movement during contrast administration, even with iodinated contrast material. Conversely, QISS MRA may provide superior image quality in segments with reduced blood flow and regions with significant calcified plaque burden. These findings underscore QISS MRA's reliability as a diagnostic alternative for lower extremity arterial imaging, offering DSA-equivalent image quality without the risks of invasive procedures and contrast agent use.

Table 11: Advantages and disadvantages of QISS MRA, CO_2 DSA, and iodinated contrast DSA. (CO_2: carbon dioxide, DSA: digital subtraction angiography; QISS MRA: Quiescent-Interval Single-Shot Magnetic Resonance Angiography)

	QISS MRA	**CO_2 DSA**	**Iodinated DSA**
Advantages	-Noninvasive -No need for contrast material -3D image reconstruction -Flow-independent assessment	-High resolution -Fast - Can be used in renal impairment	-High resolution -Fast -Widely available
Disadvantages	-Limited assessment of vessel wall -Relatively long scan time -Prone to susceptibility artifacts -Image quality may be hindered in those with irregular heart rate -Claustrophobia -Non-MRI conditional devices	-Invasive -Limited assessment of vessel wall -Cannot be used in COPD -Painful -Potential side effects such as nausea, abdominal discomfort -Flow-sensitive -Image quality can be hindered by intestinal gases	-Invasive -Requires iodinated contrast material -Limited assessment of vessel wall -Flow-sensitive

DOI:10.14753/SE.2024.3024

Figure 14: QISS MRA (A, B) and CO_2 DSA (C, D) images of the popliteal and crural region. In CO_2 DSA, reduced arterial flow prevents the contrast agent from reaching the tibioperoneal vessels, while QISS MRA shows patency in the below-the-knee region. (CO_2: carbon dioxide, DSA: digital subtraction angiography; QISS MRA: Quiescent-Interval Single-Shot Magnetic Resonance Angiography)

Figure 15: Iodinated contrast DSA (A, B, C, D) and QISS MRA (E) images reveal bilateral iliofemoral occlusion and severe stenosis. In the left leg, slowed flow parameters in DSA images prevent contrast material from reaching distal regions, while QISS MRA maintains excellent image quality. (*DSA: digital subtraction angiography; QISS MRA: Quiescent-Interval Single-Shot Magnetic Resonance Angiography)*

DOI:10.14753/SE.2024.3024

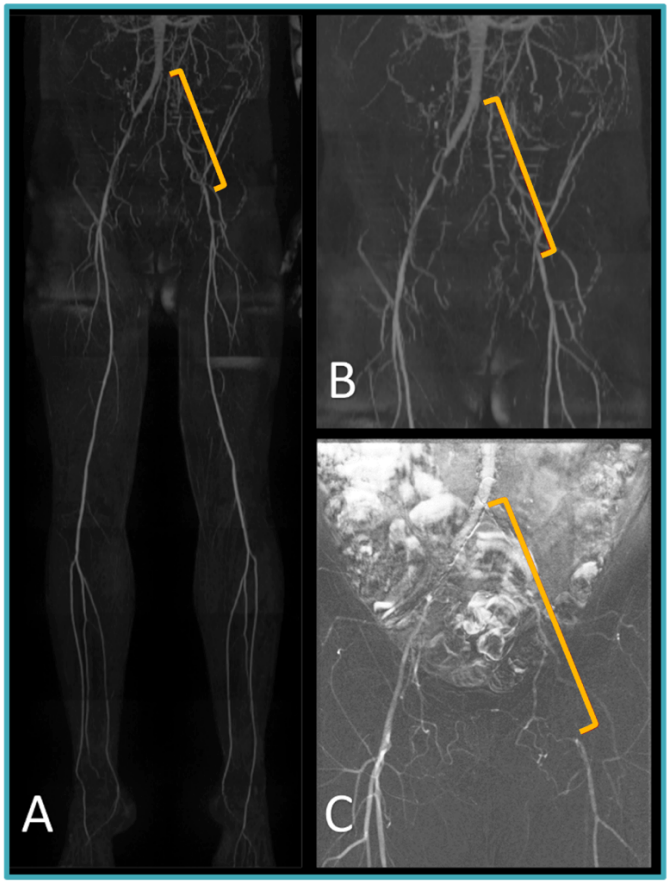

Figure 16: Comparison of Quiescent-Interval Single-Shot Magnetic Resonance Angiography (QISS MRA; A, B); and carbon dioxide digital subtraction angiography (CO_2 DSA; C) images. QISS MRA images clearly show the occlusion of the left common and external iliac artery and the resulting collateralization (yellow bracket). Assessment of this region with CO_2 DSA is severely compromised by bowel movements and intestinal gases.

5.2. Artificial intelligence in PAD plaque analysis

In our study, we investigated the feasibility of employing a semi-automated AI algorithm for tissue classification within a specific MRI histology protocol designed to visualize and categorize PAD lesion components. Our VAE algorithm demonstrated the capability to classify hard and soft tissue properties.

Choosing the appropriate revascularization method to maintain blood flow in obstructed vessels is critical for preventing amputation and mortality in PAD patients. The landmark BEST-CLI trial (2022)(142) has reshaped the landscape of PAD treatment, demonstrating improved outcomes with open surgical bypass over PVI. However, this trial also

uncovered critical gaps that, if addressed, could improve PVI outcomes. The recent, smaller landmark BASIL-2 trial (2023) (143) focusing on below-the-knee vessels showed improved outcomes with an endovascular-first approach. Both trials ultimately pointed to the importance of patient selection. Current approaches to identifying the optimal intervention and devices during intervention are subjective and inadequate. This lack of scientific knowledge is a frustrating gap for clinicians when making treatment decisions (40). The presence and extent of hard tissue pose technical challenges for existing endovascular treatment approaches compared to soft tissue components (101). Conventional clinical vascular imaging techniques, like CTA or ultrasound, currently face limitations in the visualization of tissue components within PAD lesions, primarily due to constraints in delineating soft tissue contrasts beyond calcium presence and resulting artifacts (144, 145). MRI stands out with its unique ability to evaluate soft tissue for atherosclerotic lesions, making it the ideal methodology for this purpose (97, 101, 146). However, interpretation of complex MRI scans, especially when utilizing multiple image contrasts can pose a challenge for untrained physicians. Widely employed AI algorithms like VAEs offer the advantage of rapid and automated classification once they have been adequately trained. The utilization of a substantial dataset comprising thousands of images contributes to the successful training of these algorithms. AI-supported analysis for characterizing and classifying plaque tissue in multimodality carotid and coronary artery imaging has already demonstrated its precision and robustness, providing valuable support for clinical decision-making (147). In our feasibility study, we developed an approach of obtaining several hundred images from one PAD lesion. Peripheral arterial plaques are complex and present unique challenges to visualize. Plaques consist of lipids, smooth muscle, thrombus, dense collagen, and calcium. These components and their spatial distribution impact PVI success (97, 101, 145, 148, 149). While recent advancements in MRI technology, such as QISS MRA, have enabled us to visualize the entire lower extremity arterial system without the need for contrast agents, accurately characterizing plaques remains a challenge using various imaging techniques. In severe cases, like CLTI, the composition of lesions becomes progressively more complex and covers a large spatial area, which can be effectively examined using high-resolution MRI imaging. Novel MRI-based imaging techniques overcome key limitations of current clinical imaging modalities in identifying the distribution of rigidity within a plaque (97,

101). The data resulting from a combined UTE-T2w MRI histology protocol allows precise characterization of soft/hard plaque components; it has been validated ex vivo to determine the imaging signatures of plaque components and correlation with guidewire puncture force testing to identify plaques that are difficult to penetrate (101). Furthermore, the feasibility of using the same MRI histology protocol to identify patients who were more difficult to penetrate with a guidewire during PVI was also reported in a pilot patient study in vivo (97).

Consecutive slices, acquired at a high spatial resolution and oriented perpendicular to the lesion centerline, contain a diverse range of tissue compositions, encompassing both soft and hard tissues. This results in the availability of hundreds of images per lesion for inclusion in the analysis algorithm. Thus, in our study setup, a relatively small number of lesions (five) proved sufficient to achieve well-suited image reconstructions and a clear distinction of the classes in question—specifically, the presence and quantity of soft and hard tissue components. By predefining the extent of the color space as the input to the VAE, the volume of training data required for successful semi-supervised classification with the AI algorithm is reduced, along with its design complexity. The 2D convolutional layers, forming the latent space, conform to the standard structure of a 2D CNN. Parameters for each layer, including kernel and stride sizes, as well as layer depths, were optimized to achieve the best reconstruction of the original pseudo-color RGB images. When the boundaries defining clusters within the latent space are non-linear, it can pose a challenge to effectively distinguish these clusters within a two-dimensional latent space. In such scenarios, employing a higher-dimensional latent space might be a more practical and advantageous approach. However, in our dataset, images encompassed only two classes of interest—specifically, the presence of soft and/or hard tissue. With this limited number of classes, the utilization of the VAE algorithm and a 2D latent space proved sufficient for the intended image classification, as evident from the well-separated reconstructed images produced by the trained VAE. While a 2D latent space may offer limited representation capacity compared to higher-dimensional alternatives, we aimed to demonstrate its ability to capture essential data features and variations. Adopting a higher-dimensional latent space could introduce increased complexity, necessitate more training data, and heighten the risk of overfitting. Striking a balance between the dimensionality of the latent space, model capacity, and the available data resources is

crucial. It is important to note that the dimensionality of the latent space is not fixed and can be expanded if needed. Additionally, the use of a decoder arm proves beneficial in capturing vital details and characteristics from the original data, including tissue-specific information. While the latent space provides a low-dimensional representation of the input data, it may not inherently correspond to specific classes or tissue types in the context of medical imaging data. Through training the VAE to faithfully reconstruct the input, the decoder becomes adept at extracting pertinent features for tissue classification. When combined with appropriate loss functions and training procedures, this approach aids in shaping a latent space representation with improved class separability.

Employing the classification derived from the latent space for the lesions yielded local tissue scores that aligned well with the initial visual assessment. These assessments considered aspects such as the presence of patent lumen and mild stenosis (lesion sample #1), predominantly or partially patent lumen (lesion samples #2, #3, and #5), and complex lesion composition (lesion #4). It is worth noting that the tissue score identified by the AI algorithm for a region primarily occluded by hard tissue was situated between two areas predominantly occluded by soft tissue. This observation could potentially reflect the progression of PAD lesions from simple (lesion #1) to complex (lesion #4). In addition to the demonstrated feasibility described earlier, further assessment of this algorithm is warranted, especially when extending its application to a broader range of lesions and tissue types. UTE imaging has exhibited sensitivity in distinguishing calcium from other tissues with short T2 relaxation values, which typically lack discernible intensity in conventional T1w or T2w images. Although additional validation of the color mapping to tissues, as presented here, may be considered, our feasibility study established that tissues showing signal in UTE but not in traditional T1w and T2w contrasts can be distinctly identified due to the separation of images in the latent space of the VAE algorithm. Particularly, the AI algorithm VAE is well-suited for distinguishing between hard and soft tissue types and pinpointing their locations within a PAD lesion imaged using a dedicated high-resolution MRI histology protocol.

Limitations

1. Our study on the comparison of CO_2 DSA and QISS MRA was a single-center study with a relatively small number of patients. We had a slightly higher proportion of women in our patient population, which may bias our results. We also considered CO_2 DSA as the reference standard, which has often proved to be of limited diagnostic value in the tibioperoneal region—thus using iodinated contrast agent DSA could have served as a better reference standard.

2. Our study comparing iodinated contrast DSA and QISS MRA was also conducted at a single-center and involved a relatively small patient population.

3. One notable limitation in our AI-aided plaque analysis study is the relatively small number of lesions included. While this quantity of lesions provided sufficient training data for the VAE, expanding the dataset with more lesions and images could result in a more well-defined distribution of data within the latent space. Retraining the VAE with a larger dataset may enhance the quality of the reconstructed images and classification accuracy. Moreover, expanding the color space in the RGB images may refine the classification, possibly allowing for automated assessment of free lumen as a rapid method for intervention planning. Notably, this method represents a "semi-objective" measure of feasibility. In the future, incorporating additional objective factors could further strengthen the robustness of our findings.

6. Conclusions

The conventional iodinated DSA technique, typically used in everyday clinical practice to assess lower extremity arterial disease in PAD patients with chronic renal failure, significantly elevates the risk of developing contrast-induced nephropathy (CIN). To mitigate this risk, iodinated contrast agents are substituted with carbon dioxide gas for imaging these patients. However, this substitution notably decreases image quality and diagnostic reliability. QISS MRA, as a nephroprotective and non-invasive imaging method, has the potential to address these issues.

QISS MRA consistently delivered excellent image quality in comparison to both iodinated and CO_2 contrast studies, with the highest image quality observed in the tibioperoneal region. Our findings suggest that 1.5T QISS MRA could serve as a valuable alternative for individuals for whom the use of iodinated or gadolinium contrast agents is contraindicated. This non-invasive method, non-contrast, holds relevance even for patients with normal renal function. By harnessing the potential of this technique, the diagnostic burden on patients can be further minimized, potentially leading to earlier disease detection and a reduction in the long-term risk of cardiovascular complications.

In our feasibility study on AI-aided plaque analysis, we demonstrated a novel application of a Variational Autoencoder algorithm combined with 2D convolutional networks for analyzing multi-contrast MRI images. Our custom implementation successfully sorted relevant image features, specifically the presence or absence of hard and soft tissue types, within the latent space. It is strongly advised and promising for future projects to extend the algorithm and validate its performance using supervised classification techniques. This would bolster the algorithm's capabilities and offer a more thorough assessment of its effectiveness. Additionally, the combination of AI algorithms and MRI histology holds the potential to assist clinicians in personalizing device selection and improving treatment planning.

Enhancing our understanding of diagnostic techniques for PAD is vital for making informed therapeutic decisions. Leveraging MRI advancements and integrating artificial intelligence into this intricate imaging process can usher in substantial improvements in understanding, diagnosing, and treating PAD effectively.

DOI:10.14753/SE.2024.3024

7. Summary

Introduction: PAD is often associated with impaired renal function, underscoring the necessity for nephroprotective modalities in assessment. Our study compared iodinated contrast DSA and CO_2 DSA with non-contrast QISS MRA. We also assessed the feasibility of a custom VAE using 2D CNNs on 7T MRI images to differentiate soft vs. hard plaque components in PAD.

Methods: Patients underwent elective iodinated or CO2 contrast DSA and 1.5T QISS MRA. Stenoses and image quality were evaluated. Inter-rater reliability was calculated using ICC. Diagnostic accuracy and interpretability of the modalities were assessed. VAE was evaluated on 7T MRI scans of amputated lower extremities utilizing tissue scores and classes (Class I: lumen patent, score 0; II: lumen partially patent, score 1; III: lumen mostly occluded with soft tissue, score 3, IV: mostly occluded with hard tissue, score 5)

Results: We analyzed 34 patients (623 segments) for iodinated DSA vs. QISS MRA and 28 patients (523 segments) for CO2 DSA vs. QISS MRA. QISS MRA demonstrated superior image quality over CO2 DSA in all regions ($p<0.001$) and was comparable in image quality to iodinated DSA while surpassing both in interpretability ($p<0.001$). Compared to iodinated DSA, diagnostic accuracy parameters for QISS MRA were: diagnostic accuracy 91.3%, sensitivity 84.8%, specificity 93.0%, PPV 76.3%, NPV 95.8%. Compared to CO2 DSA, QISS MRA had a diagnostic accuracy of 91.1%, sensitivity 77.8%, specificity 95.2%, PPV 83.2%, NPV 93.3%. Interobserver variability for stenosis assessment in all regions combined was 0.94 for QISS MRA and 0.88 for iodinated DSA; for QISS MRA and CO2 DSA, it was 0.97 and 0.82, respectively ($p<0.001$). We utilized 2390 MPR reconstructed MRI images to train our algorithm. Relative percentage of average tissue score varied from completely patent (lesion #1) to the presence of all four tissue classes. Lesions #2, #3 and #5 were classified to contain all tissue classes except Tissue Class IV, while lesion #4 contained all classes. Training the VAE was successful, as images with soft/hard tissues in PAD lesions were satisfactorily separated in latent space.

Conclusion: QISS MRA is a reliable and safe modality for PAD imaging. Also, using VAE may assist in rapid classification of MRI histology images acquired in a clinical setup for facilitating therapeutic decision-making.

8. References

Figure 1, 4, 10, and 11 were created by Judit Csőre.
For Figure 2, 3, 5, 12, 15, 16 image datasets were acquired at Heart and Vascular Center, Semmelweis University, Budapest, Hungary. Figures created by Judit Csőre.
Figure 6, 7, 8, 9, 13 image datasets were acquired at Houston Methodist Hospital, Houston, Texas, USA. Figures created by Judit Csőre.

1.Hiatt WR, Goldstone J, Smith SC, Jr., McDermott M, Moneta G, Oka R, Newman AB, Pearce WH. Atherosclerotic Peripheral Vascular Disease Symposium II: nomenclature for vascular diseases. Circulation. 2008;118(25):2826-2829.
2.Aboyans V, Ricco JB, Bartelink MEL, Björck M, Brodmann M, Cohnert T, Collet JP, Czerny M, De Carlo M, Debus S, Espinola-Klein C, Kahan T, Kownator S, Mazzolai L, Naylor AR, Roffi M, Röther J, Sprynger M, Tendera M, Tepe G, Venermo M, Vlachopoulos C, Desormais I. 2017 ESC Guidelines on the Diagnosis and Treatment of Peripheral Arterial Diseases, in collaboration with the European Society for Vascular Surgery (ESVS): Document covering atherosclerotic disease of extracranial carotid and vertebral, mesenteric, renal, upper and lower extremity arteriesEndorsed by: the European Stroke Organization (ESO)The Task Force for the Diagnosis and Treatment of Peripheral Arterial Diseases of the European Society of Cardiology (ESC) and of the European Society for Vascular Surgery (ESVS). Eur Heart J. 2018;39(9):763-816.
3.Eid MA, Mehta KS, Goodney PP. Epidemiology of peripheral artery disease. Seminars in Vascular Surgery. 2021;34(1):38-46.
4.Fowkes FG, Rudan D, Rudan I, Aboyans V, Denenberg JO, McDermott MM, Norman PE, Sampson UK, Williams LJ, Mensah GA, Criqui MH. Comparison of global estimates of prevalence and risk factors for peripheral artery disease in 2000 and 2010: a systematic review and analysis. Lancet. 2013;382(9901):1329-1340.
5.Roth GA, Mensah GA, Johnson CO, Addolorato G, Ammirati E, Baddour LM, Barengo NC, Beaton AZ, Benjamin EJ, Benziger CP, Bonny A, Brauer M, Brodmann M, Cahill TJ, Carapetis J, Catapano AL, Chugh SS, Cooper LT, Coresh J, Criqui M, DeCleene N, Eagle KA, Emmons-Bell S, Feigin VL, Fernández-Solà J, Fowkes G, Gakidou E, Grundy SM, He FJ, Howard G, Hu F, Inker L, Karthikeyan G, Kassebaum N, Koroshetz W, Lavie

C, Lloyd-Jones D, Lu HS, Mirijello A, Temesgen AM, Mokdad A, Moran AE, Muntner P, Narula J, Neal B, Ntsekhe M, Moraes de Oliveira G, Otto C, Owolabi M, Pratt M, Rajagopalan S, Reitsma M, Ribeiro ALP, Rigotti N, Rodgers A, Sable C, Shakil S, Sliwa-Hahnle K, Stark B, Sundström J, Timpel P, Tleyjeh IM, Valgimigli M, Vos T, Whelton PK, Yacoub M, Zuhlke L, Murray C, Fuster V. Global Burden of Cardiovascular Diseases and Risk Factors, 1990-2019: Update From the GBD 2019 Study. J Am Coll Cardiol. 2020;76(25):2982-3021.

6.Song P, Rudan D, Zhu Y, Fowkes FJI, Rahimi K, Fowkes FGR, Rudan I. Global, regional, and national prevalence and risk factors for peripheral artery disease in 2015: an updated systematic review and analysis. Lancet Glob Health. 2019;7(8):e1020-e1030.

7.Criqui MH, Matsushita K, Aboyans V, Hess CN, Hicks CW, Kwan TW, McDermott MM, Misra S, Ujueta F. Lower Extremity Peripheral Artery Disease: Contemporary Epidemiology, Management Gaps, and Future Directions: A Scientific Statement From the American Heart Association. Circulation. 2021;144(9):e171-e191.

8.Agnelli G, Belch JJF, Baumgartner I, Giovas P, Hoffmann U. Morbidity and mortality associated with atherosclerotic peripheral artery disease: A systematic review. Atherosclerosis. 2020;293:94-100.

9.Dua A, Desai SS, Patel B, Seabrook GR, Brown KR, Lewis B, Rossi PJ, Malinowski M, Lee CJ. Preventable Complications Driving Rising Costs in Management of Patients with Critical Limb Ischemia. Ann Vasc Surg. 2016;33:144-148.

10.Butnariu LI, Gorduza EV, Florea L, Țarcă E, Moisă Ș M, Tradafir LM, Cojocaru E, Luca AC, Stătescu L, Bădescu MC. The Genetic Architecture of the Etiology of Lower Extremity Peripheral Artery Disease: Current Knowledge and Future Challenges in the Era of Genomic Medicine. Int J Mol Sci. 2022;23(18).

11.Belkin N, Damrauer SM. Peripheral Arterial Disease Genetics: Progress to Date and Challenges Ahead. Curr Cardiol Rep. 2017;19(12):131.

12.Saini SK, Pérez-Cremades D, Cheng HS, Kosmac K, Peterson CA, Li L, Tian L, Dong G, Wu KK, Bouverat B, Wohlgemuth SE, Ryan T, Sufit RL, Ferrucci L, McDermott MM, Leeuwenburgh C, Feinberg MW. Dysregulated Genes, MicroRNAs, Biological Pathways, and Gastrocnemius Muscle Fiber Types Associated With Progression of Peripheral Artery Disease: A Preliminary Analysis. J Am Heart Assoc. 2022;11(21):e023085.

13.Gerhard-Herman MD, Gornik HL, Barrett C, Barshes NR, Corriere MA, Drachman DE, Fleisher LA, Fowkes FG, Hamburg NM, Kinlay S, Lookstein R, Misra S, Mureebe L, Olin JW, Patel RA, Regensteiner JG, Schanzer A, Shishehbor MH, Stewart KJ, Treat-Jacobson D, Walsh ME. 2016 AHA/ACC Guideline on the Management of Patients With Lower Extremity Peripheral Artery Disease: A Report of the American College of Cardiology/American Heart Association Task Force on Clinical Practice Guidelines. Circulation. 2017;135(12):e726-e779.

14.Nordanstig J, Behrendt C-A, Baumgartner I, Belch J, Bäck M, Fitridge R, Hinchliffe R, Lejay A, Mills JL, Rother U, Sigvant B, Spanos K, Szeberin Z, van de Water W, Antoniou GA, Björck M, Gonçalves FB, Coscas R, Dias NV, Van Herzeele I, Lepidi S, Mees BME, Resch TA, Ricco J-B, Trimarchi S, Twine CP, Tulamo R, Wanhainen A, Boyle JR, Brodmann M, Dardik A, Dick F, Goëffic Y, Holden A, Kakkos SK, Kolh P, McDermott MM. Editor's Choice -- European Society for Vascular Surgery (ESVS) 2024 Clinical Practice Guidelines on the Management of Asymptomatic Lower Limb Peripheral Arterial Disease and Intermittent Claudication[☆]. European Journal of Vascular and Endovascular Surgery. 2024;67(1):9-96.

15.Aday AW, Matsushita K. Epidemiology of Peripheral Artery Disease and Polyvascular Disease. Circulation Research. 2021;128(12):1818-1832.

16.Norgren L, Hiatt WR, Dormandy JA, Nehler MR, Harris KA, Fowkes FG. Inter-Society Consensus for the Management of Peripheral Arterial Disease (TASC II). J Vasc Surg. 2007;45 Suppl S:S5-67.

17.Hirsch AT, Allison MA, Gomes AS, Corriere MA, Duval S, Ershow AG, Hiatt WR, Karas RH, Lovell MB, McDermott MM, Mendes DM, Nussmeier NA, Treat-Jacobson D. A call to action: women and peripheral artery disease: a scientific statement from the American Heart Association. Circulation. 2012;125(11):1449-1472.

18.Joosten MM, Pai JK, Bertoia ML, Rimm EB, Spiegelman D, Mittleman MA, Mukamal KJ. Associations between conventional cardiovascular risk factors and risk of peripheral artery disease in men. Jama. 2012;308(16):1660-1667.

19.Kannel WB, McGee DL. Update on some epidemiologic features of intermittent claudication: the Framingham Study. J Am Geriatr Soc. 1985;33(1):13-18.

20.Murabito JM, D'Agostino RB, Silbershatz H, Wilson WF. Intermittent claudication. A risk profile from The Framingham Heart Study. Circulation. 1997;96(1):44-49.

21.Jude EB, Oyibo SO, Chalmers N, Boulton AJ. Peripheral arterial disease in diabetic and nondiabetic patients: a comparison of severity and outcome. Diabetes Care. 2001;24(8):1433-1437.
22.Abbott RD, Brand FN, Kannel WB. Epidemiology of some peripheral arterial findings in diabetic men and women: experiences from the Framingham Study. Am J Med. 1990;88(4):376-381.
23.Soyoye DO, Abiodun OO, Ikem RT, Kolawole BA, Akintomide AO. Diabetes and peripheral artery disease: A review. World J Diabetes. 2021;12(6):827-838.
24.Barnes JA, Eid MA, Creager MA, Goodney PP. Epidemiology and Risk of Amputation in Patients With Diabetes Mellitus and Peripheral Artery Disease. Arterioscler Thromb Vasc Biol. 2020;40(8):1808-1817.
25.Layden J, Michaels J, Bermingham S, Higgins B. Diagnosis and management of lower limb peripheral arterial disease: summary of NICE guidance. Bmj. 2012;345:e4947.
26.Gheith O, Farouk N, Nampoory N, Halim MA, Al-Otaibi T. Diabetic kidney disease: world wide difference of prevalence and risk factors. J Nephropharmacol. 2016;5(1):49-56.
27.Tunstall-Pedoe H, Peters SAE, Woodward M, Struthers AD, Belch JJF. Twenty-Year Predictors of Peripheral Arterial Disease Compared With Coronary Heart Disease in the Scottish Heart Health Extended Cohort (SHHEC). J Am Heart Assoc. 2017;6(9).
28.Masoura C, Pitsavos C, Aznaouridis K, Skoumas I, Vlachopoulos C, Stefanadis C. Arterial endothelial function and wall thickness in familial hypercholesterolemia and familial combined hyperlipidemia and the effect of statins. A systematic review and meta-analysis. Atherosclerosis. 2011;214(1):129-138.
29.Akioyamen LE, Tu JV, Genest J, Ko DT, Coutin AJS, Shan SD, Chu A. Risk of Ischemic Stroke and Peripheral Arterial Disease in Heterozygous Familial Hypercholesterolemia: A Meta-Analysis. Angiology. 2019;70(8):726-736.
30.Kontush A. HDL and Reverse Remnant-Cholesterol Transport (RRT): Relevance to Cardiovascular Disease. Trends Mol Med. 2020;26(12):1086-1100.
31.Aday AW, Lawler PR, Cook NR, Ridker PM, Mora S, Pradhan AD. Lipoprotein Particle Profiles, Standard Lipids, and Peripheral Artery Disease Incidence. Circulation. 2018;138(21):2330-2341.

32.Willigendael EM, Teijink JA, Bartelink ML, Kuiken BW, Boiten J, Moll FL, Büller HR, Prins MH. Influence of smoking on incidence and prevalence of peripheral arterial disease. J Vasc Surg. 2004;40(6):1158-1165.
33.Olin JW, Sealove BA. Peripheral artery disease: current insight into the disease and its diagnosis and management. Mayo Clin Proc. 2010;85(7):678-692.
34.Tummala S, Scherbel D. Clinical Assessment of Peripheral Arterial Disease in the Office: What Do the Guidelines Say? Semin Intervent Radiol. 2018;35(5):365-377.
35.Diehm C, Allenberg JR, Pittrow D, Mahn M, Tepohl G, Haberl RL, Darius H, Burghaus I, Trampisch HJ. Mortality and vascular morbidity in older adults with asymptomatic versus symptomatic peripheral artery disease. Circulation. 2009;120(21):2053-2061.
36.Dhaliwal G, Mukherjee D. Peripheral arterial disease: Epidemiology, natural history, diagnosis and treatment. Int J Angiol. 2007;16(2):36-44.
37.Schainfeld RM. Management of peripheral arterial disease and intermittent claudication. J Am Board Fam Pract. 2001;14(6):443-450.
38.Simon RW, Simon-Schulthess A, Amann-Vesti BR. Intermittent claudication. Bmj. 2007;334(7596):746.
39.Morley RL, Sharma A, Horsch AD, Hinchliffe RJ. Peripheral artery disease. Bmj. 2018;360:j5842.
40.Conte MS, Bradbury AW, Kolh P, White JV, Dick F, Fitridge R, Mills JL, Ricco JB, Suresh KR, Murad MH, Aboyans V, Aksoy M, Alexandrescu VA, Armstrong D, Azuma N, Belch J, Bergoeing M, Bjorck M, Chakfé N, Cheng S, Dawson J, Debus ES, Dueck A, Duval S, Eckstein HH, Ferraresi R, Gambhir R, Gargiulo M, Geraghty P, Goode S, Gray B, Guo W, Gupta PC, Hinchliffe R, Jetty P, Komori K, Lavery L, Liang W, Lookstein R, Menard M, Misra S, Miyata T, Moneta G, Munoa Prado JA, Munoz A, Paolini JE, Patel M, Pomposelli F, Powell R, Robless P, Rogers L, Schanzer A, Schneider P, Taylor S, De Ceniga MV, Veller M, Vermassen F, Wang J, Wang S. Global Vascular Guidelines on the Management of Chronic Limb-Threatening Ischemia. Eur J Vasc Endovasc Surg. 2019;58(1s):S1-S109.e133.
41.McDermott MM, Greenland P, Liu K, Guralnik JM, Criqui MH, Dolan NC, Chan C, Celic L, Pearce WH, Schneider JR, Sharma L, Clark E, Gibson D, Martin GJ. Leg

symptoms in peripheral arterial disease: associated clinical characteristics and functional impairment. Jama. 2001;286(13):1599-1606.

42.McDermott MM. Lower extremity manifestations of peripheral artery disease: the pathophysiologic and functional implications of leg ischemia. Circ Res. 2015;116(9):1540-1550.

43.Fontaine R. Surgical treatment of peripheral circulation disorders. Helv Chir Acta. 1954;21:499-533.

44.Rutherford RB, Baker JD, Ernst C, Johnston KW, Porter JM, Ahn S, Jones DN. Recommended standards for reports dealing with lower extremity ischemia: revised version. Journal of vascular surgery. 1997;26(3):517-538.

45.Dormandy JA. Management of peripheral arterial disease (PAD). TASC working group. TransAtlantic inter-society consensus (TASC). J Vasc surg. 2000;31:S1-S296.

46.Wijnand JGJ, Zarkowsky D, Wu B, van Haelst STW, Vonken EPA, Sorrentino TA, Pallister Z, Chung J, Mills JL, Teraa M, Verhaar MC, de Borst GJ, Conte MS. The Global Limb Anatomic Staging System (GLASS) for CLTI: Improving Inter-Observer Agreement. J Clin Med. 2021;10(16).

47.Akai T, Yamamoto K, Okamoto H, Shigematsu K, Otsu H, Watanabe T, Miyata T. Usefulness of the Bollinger scoring method in evaluating peripheral artery angiography with 64-low computed tomography in patients with peripheral arterial disease. Int Angiol. 2014;33(5):426-433.

48.Mills Sr JL, Conte MS, Armstrong DG, Pomposelli FB, Schanzer A, Sidawy AN, Andros G, Committee SfVSLEG. The society for vascular surgery lower extremity threatened limb classification system: risk stratification based on wound, ischemia, and foot infection (WIfI). Journal of vascular surgery. 2014;59(1):220-234. e222.

49.Cerqueira LO, Duarte EG, Barros ALS, Cerqueira JR, de Araújo WJB. WIfI classification: the Society for Vascular Surgery lower extremity threatened limb classification system, a literature review. J Vasc Bras. 2020;19:e20190070.

50.Fowkes F, Murray G, Butcher I, Heald C, Lee R, Chambless L, Folsom A, Hirsch A, Dramaix M, deBacker G. Ankle Brachial Index Collaboration: Ankle brachial index combined with Framingham Risk Score to predict cardiovascular events and mortality: a meta-analysis. JAMA. 2008;300(2):197-208.

51.Weinberg I, Giri J, Calfon MA, Hawkins BM, Weinberg MD, Margey R, Hannon K, Schainfeld RM, Jaff MR. Anatomic correlates of supra-normal ankle brachial indices. Catheter Cardiovasc Interv. 2013;81(6):1025-1030.

52.Sorensen J, Wilks SA, Jacob AD, Huynh TT. Screening for peripheral artery disease. Semin Roentgenol. 2015;50(2):139-147.

53.Martinelli O, Alunno A, Jabbour J, Cuozzo S, Gattuso R. Duplex ultrasound as a reliable alternative to CT angiography for treatment planning of peripheral artery disease. Int Angiol. 2021;40(4):306-314.

54.Tummala S, Richardson AJ. Infrapopliteal Artery Chronic Total Occlusion Crossing Techniques: An Overview for Endovascular Specialists. Semin Intervent Radiol. 2021;38(4):492-499.

55.Cires-Drouet RS, Mozafarian M, Ali A, Sikdar S, Lal BK. Imaging of high-risk carotid plaques: ultrasound. Semin Vasc Surg. 2017;30(1):44-53.

56.Khan AA, Koudelka C, Goldstein C, Zhao L, Yokemick J, Dux M, Sikdar S, Lal BK. Semiautomatic quantification of carotid plaque volume with three-dimensional ultrasound imaging. J Vasc Surg. 2017;65(5):1407-1417.

57.Crawford JD, Robbins NG, Harry LA, Wilson DG, McLafferty RB, Mitchell EL, Landry GJ, Moneta GL. Characterization of tibial velocities by duplex ultrasound in severe peripheral arterial disease and controls. J Vasc Surg. 2016;63(3):646-651.

58.Dias-Neto M, Marques C, Sampaio S. Digital Subtraction Angiography or Computed Tomography Angiography in the Preoperative Evaluation of Lower Limb Peripheral Artery Disease - A Comparative Analysis. Rev Port Cir Cardiotorac Vasc. 2017;24(3-4):174.

59.Gyánó M, Csobay-Novák C, Berczeli M, Góg I, Kiss JP, Szigeti K, Osváth S, Nemes B. Initial Operating Room Experience with Digital Variance Angiography in Carbon Dioxide-Assisted Lower Limb Interventions: A Pilot Study. Cardiovasc Intervent Radiol. 2020;43(8):1226-1231.

60.Thomas RP, Viniol S, König AM, Portig I, Swaid Z, Mahnken AH. Feasibility and safety of automated CO2 angiography in peripheral arterial interventions. Medicine (Baltimore). 2021;100(2):e24254.

61.Prasad A. CO2 angiography for peripheral arterial imaging: the good, bad, and ugly. Catheter Cardiovasc Interv. 2015;85(5):878-879.

62.Cho KJ. Carbon Dioxide Angiography: Scientific Principles and Practice. Vasc Specialist Int. 2015;31(3):67-80.
63.Sharafuddin MJ, Marjan AE. Current status of carbon dioxide angiography. J Vasc Surg. 2017;66(2):618-637.
64.Zettervall SL, Marshall AP, Fleser P, Guzman RJ. Association of arterial calcification with chronic limb ischemia in patients with peripheral artery disease. J Vasc Surg. 2018;67(2):507-513.
65.Fleischmann D, Lammer J. Peripheral CT angiography for interventional treatment planning. Eur Radiol. 2006;16 Suppl 7:M58-64.
66.Heijenbrok-Kal MH, Kock MC, Hunink MG. Lower extremity arterial disease: multidetector CT angiography meta-analysis. Radiology. 2007;245(2):433-439.
67.Saphir E, Svensson-Björk R, Acosta S. Performance of Computed Tomography Angiography Before Revascularization Is Associated With Higher Amputation-Free Survival in Rutherford IIb Acute Lower Limb Ischaemia. Front Surg. 2021;8:744721.
68.Kosmala A, Weng AM, Schmid A, Gruschwitz P, Grunz JP, Bley TA, Petritsch B. Dual-Energy CT Angiography in Peripheral Arterial Occlusive Disease: Diagnostic Accuracy of Different Image Reconstruction Approaches. Acad Radiol. 2022;29 Suppl 4:S59-s68.
69.Mergen V, Eberhard M, Manka R, Euler A, Alkadhi H. First in-human quantitative plaque characterization with ultra-high resolution coronary photon-counting CT angiography. Front Cardiovasc Med. 2022;9:981012.
70.Roy TL, Forbes TL, Dueck AD, Wright GA. MRI for peripheral artery disease: Introductory physics for vascular physicians. Vasc Med. 2018;23(2):153-162.
71.Khairnar S, More N, Mounika C, Kapusetti G. Advances in Contrast Agents for Contrast-Enhanced Magnetic Resonance Imaging. J Med Imaging Radiat Sci. 2019;50(4):575-589.
72.Chan D, Anderson ME, Dolmatch BL. Imaging evaluation of lower extremity infrainguinal disease: role of the noninvasive vascular laboratory, computed tomography angiography, and magnetic resonance angiography. Tech Vasc Interv Radiol. 2010;13(1):11-22.
73.Jens S, Koelemay MJW, Reekers JA, Bipat S. Diagnostic performance of computed tomography angiography and contrast-enhanced magnetic resonance angiography in

patients with critical limb ischaemia and intermittent claudication: systematic review and meta-analysis. European Radiology. 2013;23:3104-3114.

74.Leiner T, Bogaert J, Friedrich MG, Mohiaddin R, Muthurangu V, Myerson S, Powell AJ, Raman SV, Pennell DJ. SCMR Position Paper (2020) on clinical indications for cardiovascular magnetic resonance. Journal of Cardiovascular Magnetic Resonance. 2020;22(1):76.

75.Leiner T. Magnetic resonance angiography of abdominal and lower extremity vasculature. Top Magn Reson Imaging. 2005;16(1):21-66.

76.Swan JS, Carroll TJ, Kennell TW, Heisey DM, Korosec FR, Frayne R, Mistretta CA, Grist TM. Time-resolved three-dimensional contrast-enhanced MR angiography of the peripheral vessels. Radiology. 2002;225(1):43-52.

77.Gallo-Bernal S, Patino-Jaramillo N, Calixto CA, Higuera SA, Forero JF, Lara Fernandes J, Góngora C, Gee MS, Ghoshhajra B, Medina HM. Nephrogenic Systemic Fibrosis in Patients with Chronic Kidney Disease after the Use of Gadolinium-Based Contrast Agents: A Review for the Cardiovascular Imager. Diagnostics (Basel). 2022;12(8).

78.Thomsen HS, Morcos SK, Almén T, Bellin MF, Bertolotto M, Bongartz G, Clement O, Leander P, Heinz-Peer G, Reimer P, Stacul F, van der Molen A, Webb JA. Nephrogenic systemic fibrosis and gadolinium-based contrast media: updated ESUR Contrast Medium Safety Committee guidelines. Eur Radiol. 2013;23(2):307-318.

79.Woolen SA, Shankar PR, Gagnier JJ, MacEachern MP, Singer L, Davenport MS. Risk of Nephrogenic Systemic Fibrosis in Patients With Stage 4 or 5 Chronic Kidney Disease Receiving a Group II Gadolinium-Based Contrast Agent: A Systematic Review and Meta-analysis. JAMA Intern Med. 2020;180(2):223-230.

80.Bäuerle T, Saake M, Uder M. Gadolinium-based contrast agents: What we learned from acute adverse events, nephrogenic systemic fibrosis and brain retention. Rofo. 2021;193(9):1010-1018.

81.Toth GB, Varallyay CG, Horvath A, Bashir MR, Choyke PL, Daldrup-Link HE, Dosa E, Finn JP, Gahramanov S, Harisinghani M, Macdougall I, Neuwelt A, Vasanawala SS, Ambady P, Barajas R, Cetas JS, Ciporen J, DeLoughery TJ, Doolittle ND, Fu R, Grinstead J, Guimaraes AR, Hamilton BE, Li X, McConnell HL, Muldoon LL, Nesbit G, Netto JP, Petterson D, Rooney WD, Schwartz D, Szidonya L, Neuwelt EA. Current and

potential imaging applications of ferumoxytol for magnetic resonance imaging. Kidney Int. 2017;92(1):47-66.

82.Navot B, Hecht EM, Lim RP, Edelman RR, Koktzoglou I. MR Angiography Series: Fundamentals of Non-Contrast-enhanced MR Angiography. Radiographics. 2021;41(5):E157-e158.

83.Mihai G, Chung YC, Kariisa M, Raman SV, Simonetti OP, Rajagopalan S. Initial feasibility of a multi-station high resolution three-dimensional dark blood angiography protocol for the assessment of peripheral arterial disease. J Magn Reson Imaging. 2009;30(4):785-793.

84.Miyazaki M, Akahane M. Non-contrast enhanced MR angiography: established techniques. J Magn Reson Imaging. 2012;35(1):1-19.

85.Knobloch G, Gielen M, Lauff MT, Romano VC, Schmitt P, Rick M, Kröncke TJ, Huppertz A, Hamm B, Wagner M. ECG-gated quiescent-interval single-shot MR angiography of the lower extremities: initial experience at 3 T. Clin Radiol. 2014;69(5):485-491.

86.Kazemtash M, Harth M, Derwich W, Thalhammer A, Schmitz-Rixen T, Keese M. Quiescent-Interval Slice Selective Magnetic Resonance Angiography for Abdominal Aortic Aneurysm Treatment Planning. J Endovasc Ther. 2021;28(3):393-398.

87.Mostafa K, Pfarr J, Langguth P, Schäfer JP, Trentmann J, Koktzoglou I, Edelman RR, Bueno Neves F, Graessner J, Both M, Jansen O, Salehi Ravesh M. Clinical Evaluation of Non-Contrast-Enhanced Radial Quiescent-Interval Slice-Selective (QISS) Magnetic Resonance Angiography in Comparison to Contrast-Enhanced Computed Tomography Angiography for the Evaluation of Endoleaks after Abdominal Endovascular Aneurysm Repair. J Clin Med. 2022;11(21).

88.Edelman RR, Silvers RI, Thakrar KH, Metzl MD, Nazari J, Giri S, Koktzoglou I. Nonenhanced MR angiography of the pulmonary arteries using single-shot radial quiescent-interval slice-selective (QISS): a technical feasibility study. J Cardiovasc Magn Reson. 2017;19(1):48.

89.Ward EV, Galizia MS, Usman A, Popescu AR, Dunkle E, Edelman RR. Comparison of quiescent inflow single-shot and native space for nonenhanced peripheral MR angiography. J Magn Reson Imaging. 2013;38(6):1531-1538.

90.Knobloch G, Lauff MT, Hanke M, Schwenke C, Hamm B, Wagner M. Non-contrast-enhanced MR-angiography (MRA) of lower extremity peripheral arterial disease at 3 tesla: Examination time and diagnostic performance of 2D quiescent-interval single-shot MRA vs. 3D fast spin-Echo MRA. Magn Reson Imaging. 2021;76:17-25.
91.Saini A, Wallace A, Albadawi H, Naidu S, Alzubaidi S, Knuttinen MG, Panda A, Oklu R. Quiescent-Interval Single-Shot Magnetic Resonance Angiography. Diagnostics (Basel). 2018;8(4).
92.Edelman RR, Carr M, Koktzoglou I. Advances in non-contrast quiescent-interval slice-selective (QISS) magnetic resonance angiography. Clin Radiol. 2019;74(1):29-36.
93.Klasen J, Blondin D, Schmitt P, Bi X, Sansone R, Wittsack HJ, Kröpil P, Quentin M, Kuhlemann J, Miese F, Heiss C, Kelm M, Antoch G, Lanzman RS. Nonenhanced ECG-gated quiescent-interval single-shot MRA (QISS-MRA) of the lower extremities: comparison with contrast-enhanced MRA. Clin Radiol. 2012;67(5):441-446.
94.Carr JC. QISS MR Angiography: An Alternative to CT Angiography for Peripheral Vascular Evaluation. JACC Cardiovasc Imaging. 2017;10(10 Pt A):1125-1127.
95.Bradbury AW, Adam DJ, Bell J, Forbes JF, Fowkes FG, Gillespie I, Ruckley CV, Raab GM. Bypass versus Angioplasty in Severe Ischaemia of the Leg (BASIL) trial: Analysis of amputation free and overall survival by treatment received. J Vasc Surg. 2010;51(5 Suppl):18s-31s.
96.Farber A, Menard MT, Conte MS, Kaufman JA, Powell RJ, Choudhry NK, Hamza TH, Assmann SF, Creager MA, Cziraky MJ, Dake MD, Jaff MR, Reid D, Siami FS, Sopko G, White CJ, van Over M, Strong MB, Villarreal MF, McKean M, Azene E, Azarbal A, Barleben A, Chew DK, Clavijo LC, Douville Y, Findeiss L, Garg N, Gasper W, Giles KA, Goodney PP, Hawkins BM, Herman CR, Kalish JA, Koopmann MC, Laskowski IA, Mena-Hurtado C, Motaganahalli R, Rowe VL, Schanzer A, Schneider PA, Siracuse JJ, Venermo M, Rosenfield K. Surgery or Endovascular Therapy for Chronic Limb-Threatening Ischemia. New England Journal of Medicine. 2022;387(25):2305-2316.
97.Roy TL, Chen HJ, Dueck AD, Wright GA. Magnetic resonance imaging characteristics of lesions relate to the difficulty of peripheral arterial endovascular procedures. J Vasc Surg. 2018;67(6):1844-1854.e1842.

98.Siu AG, Ramadeen A, Hu X, Morikawa L, Zhang L, Lau JY, Liu G, Pop M, Connelly KA, Dorian P, Wright GA. Characterization of the ultrashort-TE (UTE) MR collagen signal. NMR Biomed. 2015;28(10):1236-1244.
99.Sharma S, Boujraf S, Hombach V, Ignatius A, Oberhuber A, Rasche V. Quantification of Calcifications in Endarterectomy Samples by Means of High-Resolution Ultra-Short Echo Time Imaging. Investigative radiology. 2010;45:109-113.
100.Yassin A, Pedrosa I, Kearney M, Genega E, Rofsky NM, Lenkinski RE. In vitro MR imaging of renal stones with an ultra-short echo time magnetic resonance imaging sequence. Acad Radiol. 2012;19(12):1566-1572.
101.Roy T, Liu G, Shaikh N, Dueck AD, Wright GA. Puncturing Plaques. J Endovasc Ther. 2017;24(1):35-46.
102.Gore JC. Artificial intelligence in medical imaging. Magn Reson Imaging. 2020;68:A1-a4.
103.Currie G, Hawk KE, Rohren E, Vial A, Klein R. Machine Learning and Deep Learning in Medical Imaging: Intelligent Imaging. J Med Imaging Radiat Sci. 2019;50(4):477-487.
104.Bevan GH, White Solaru KT. Evidence-Based Medical Management of Peripheral Artery Disease. Arterioscler Thromb Vasc Biol. 2020;40(3):541-553.
105.Fukushima K. Neocognitron: a self organizing neural network model for a mechanism of pattern recognition unaffected by shift in position. Biol Cybern. 1980;36(4):193-202.
106.Chatterjee S, Maity S, Bhattacharjee M, Banerjee S, Das AK, Ding W. Variational Autoencoder Based Imbalanced COVID-19 Detection Using Chest X-Ray Images. New Gener Comput. 2023;41(1):25-60.
107.Han K, Wen H, Shi J, Lu KH, Zhang Y, Fu D, Liu Z. Variational autoencoder: An unsupervised model for encoding and decoding fMRI activity in visual cortex. Neuroimage. 2019;198:125-136.
108.Zammit J, Fung DLX, Liu Q, Leung CK, Hu P. Semi-supervised COVID-19 CT image segmentation using deep generative models. BMC Bioinformatics. 2022;23(Suppl 7):343.
109.Hosny A, Parmar C, Quackenbush J, Schwartz LH, Aerts H. Artificial intelligence in radiology. Nat Rev Cancer. 2018;18(8):500-510.

110. Marino J. Predictive Coding, Variational Autoencoders, and Biological Connections. Neural Comput. 2021;34(1):1-44.
111. Ye F, Bors AG. Lifelong Mixture of Variational Autoencoders. IEEE Trans Neural Netw Learn Syst. 2021;Pp.
112. Xu W, Tan Y. Semisupervised Text Classification by Variational Autoencoder. IEEE Trans Neural Netw Learn Syst. 2020;31(1):295-308.
113. Chen J, Du L, Liao L. Discriminative Mixture Variational Autoencoder for Semisupervised Classification. IEEE Trans Cybern. 2022;52(5):3032-3046.
114. Yang Y, Zheng K, Wu C, Yang Y. Improving the Classification Effectiveness of Intrusion Detection by Using Improved Conditional Variational AutoEncoder and Deep Neural Network. Sensors. 2019;19(11):2528.
115. Csore J, Karmonik C, Wilhoit K, Buckner L, Roy TL. Automatic Classification of Magnetic Resonance Histology of Peripheral Arterial Chronic Total Occlusions Using a Variational Autoencoder: A Feasibility Study. Diagnostics. 2023;13(11):1925.
116. Armstrong EJ, Wu J, Singh GD, Dawson DL, Pevec WC, Amsterdam EA, Laird JR. Smoking cessation is associated with decreased mortality and improved amputation-free survival among patients with symptomatic peripheral artery disease. J Vasc Surg. 2014;60(6):1565-1571.
117. Lane R, Ellis B, Watson L, Leng GC. Exercise for intermittent claudication. Cochrane Database Syst Rev. 2014(7):Cd000990.
118. Bonaca MP, Nault P, Giugliano RP, Keech AC, Pineda AL, Kanevsky E, Kuder J, Murphy SA, Jukema JW, Lewis BS, Tokgozoglu L, Somaratne R, Sever PS, Pedersen TR, Sabatine MS. Low-Density Lipoprotein Cholesterol Lowering With Evolocumab and Outcomes in Patients With Peripheral Artery Disease: Insights From the FOURIER Trial (Further Cardiovascular Outcomes Research With PCSK9 Inhibition in Subjects With Elevated Risk). Circulation. 2018;137(4):338-350.
119. Vartanian SM, Conte MS. Surgical intervention for peripheral arterial disease. Circ Res. 2015;116(9):1614-1628.
120. Dayama A, Tsilimparis N, Kolakowski S, Matolo NM, Humphries MD. Clinical outcomes of bypass-first versus endovascular-first strategy in patients with chronic limb-threatening ischemia due to infrageniculate arterial disease. Journal of Vascular Surgery. 2019;69(1):156-163.e151.

121. Almasri J, Adusumalli J, Asi N, Lakis S, Alsawas M, Prokop LJ, Bradbury A, Kolh P, Conte MS, Murad MH. A systematic review and meta-analysis of revascularization outcomes of infrainguinal chronic limb-threatening ischemia. Journal of Vascular Surgery. 2018;68(2):624-633.
122. Jaff MR, White CJ, Hiatt WR, Fowkes GR, Dormandy J, Razavi M, Reekers J, Norgren L. An Update on Methods for Revascularization and Expansion of the TASC Lesion Classification to Include Below-the-Knee Arteries: A Supplement to the Inter-Society Consensus for the Management of Peripheral Arterial Disease (TASC II). Vascular Medicine. 2015;20(5):465-478.
123. Bradbury AW, Adam DJ, Bell J, Forbes JF, Fowkes FGR, Gillespie I, Ruckley CV, Raab GM. Bypass versus Angioplasty in Severe Ischaemia of the Leg (BASIL) trial: Analysis of amputation free and overall survival by treatment received. Journal of Vascular Surgery. 2010;51(5):18S-31S.
124. Popplewell MA, Davies HOB, Meecham L, Bate G, Bradbury AW. Comparison of Clinical Outcomes in Patients Selected for Infra-Popliteal Bypass or Plain Balloon Angioplasty for Chronic Limb Threatening Ischemia Between 2009 and 2013. Vasc Endovascular Surg. 2020;55(1):1538574420953949.
125. Arendt CT, Leithner D, Lenga L, Wichmann JL, Albrecht MH, Czwikla R, Varga-Szemes A, d'Angelo T, Martin SS, Thalhammer A, Nagel E, Vogl TJ, Gruber-Rouh T. Multi-observer comparison study between unenhanced quiescent-interval single-shot magnetic resonance angiography and invasive carbon dioxide angiography in patients with peripheral arterial disease and chronic renal insufficiency. Eur J Radiol. 2018;108:140-146.
126. Mishra A, Jain NK, Bhagwat A. CT Angiography of Peripheral Arterial Disease by 256-Slice Scanner: Accuracy, Advantages and Disadvantages Compared to Digital Subtraction Angiography. Vascular and Endovascular Surgery. 2017;51:247 - 254.
127. Ofer A, Nitecki SS, Linn S, Epelman M, Fischer D, Karram T, Litmanovich D, Schwartz H, Hoffman A, Engel A. Multidetector CT angiography of peripheral vascular disease: a prospective comparison with intraarterial digital subtraction angiography. AJR Am J Roentgenol. 2003;180(3):719-724.
128. Koo TK, Li MY. A Guideline of Selecting and Reporting Intraclass Correlation Coefficients for Reliability Research. J Chiropr Med. 2016;15(2):155-163.

129. Fedorov A, Beichel R, Kalpathy-Cramer J, Finet J, Fillion-Robin JC, Pujol S, Bauer C, Jennings D, Fennessy F, Sonka M, Buatti J, Aylward S, Miller JV, Pieper S, Kikinis R. 3D Slicer as an image computing platform for the Quantitative Imaging Network. Magn Reson Imaging. 2012;30(9):1323-1341.

130. National Institute for Health and Care Excellence: Guidelines. Peripheral arterial disease: diagnosis and management. London: National Institute for Health and Care Excellence (NICE)

Copyright © NICE 2020.; 2020.

131. Sarkadi H, Csőre J, Veres DS, Szegedi N, Molnár L, Gellér L, Bérczi V, Dósa E. Incidence of and predisposing factors for pseudoaneurysm formation in a high-volume cardiovascular center. PLoS One. 2021;16(8):e0256317.

132. Minici R, Paone S, Talarico M, Zappia L, Abdalla K, Petullà M, Laganà D. Percutaneous treatment of vascular access-site complications: a ten years' experience in two centres. CVIR Endovascular. 2020;3(1):29.

133. Hodnett PA, Koktzoglou I, Davarpanah AH, Scanlon TG, Collins JD, Sheehan JJ, Dunkle EE, Gupta N, Carr JC, Edelman RR. Evaluation of peripheral arterial disease with nonenhanced quiescent-interval single-shot MR angiography. Radiology. 2011;260(1):282-293.

134. Altaha MA, Jaskolka JD, Tan K, Rick M, Schmitt P, Menezes RJ, Wintersperger BJ. Non-contrast-enhanced MR angiography in critical limb ischemia: performance of quiescent-interval single-shot (QISS) and TSE-based subtraction techniques. European Radiology. 2017;27(3):1218-1226.

135. Mathur M, Jones JR, Weinreb JC. Gadolinium Deposition and Nephrogenic Systemic Fibrosis: A Radiologist's Primer. RadioGraphics. 2019;40(1):153-162.

136. Weinreb JC, Rodby RA, Yee J, Wang CL, Fine D, McDonald RJ, Perazella MA, Dillman JR, Davenport MS. Use of Intravenous Gadolinium-based Contrast Media in Patients with Kidney Disease: Consensus Statements from the American College of Radiology and the National Kidney Foundation. Radiology. 2021;298(1):28-35.

137. van der Molen AJ, Reimer P, Dekkers IA, Bongartz G, Bellin MF, Bertolotto M, Clement O, Heinz-Peer G, Stacul F, Webb JAW, Thomsen HS. Post-contrast acute kidney injury. Part 2: risk stratification, role of hydration and other prophylactic measures, patients taking metformin and chronic dialysis patients : Recommendations for updated

ESUR Contrast Medium Safety Committee guidelines. Eur Radiol. 2018;28(7):2856-2869.

138. Zhang N, Zou L, Huang Y, Liu D, Tang Y, Fan Z, Chen H, Liu X. Non-Contrast Enhanced MR Angiography (NCE-MRA) of the Calf: A Direct Comparison between Flow-Sensitive Dephasing (FSD) Prepared Steady-State Free Precession (SSFP) and Quiescent-Interval Single-Shot (QISS) in Patients with Diabetes. PLoS One. 2015;10(6):e0128786.

139. Offerman EJ, Hodnett PA, Edelman RR, Koktzoglou I. Nonenhanced methods for lower-extremity MRA: a phantom study examining the effects of stenosis and pathologic flow waveforms at 1.5T. J Magn Reson Imaging. 2011;33(2):401-408.

140. Edelman RR, Giri S, Murphy IG, Flanagan O, Speier P, Koktzoglou I. Ungated radial quiescent-inflow single-shot (UnQISS) magnetic resonance angiography using optimized azimuthal equidistant projections. Magn Reson Med. 2014;72(6):1522-1529.

141. Varga-Szemes A, Penmetsa M, Emrich T, Todoran TM, Suranyi P, Fuller SR, Edelman RR, Koktzoglou I, Schoepf UJ. Diagnostic accuracy of non-contrast quiescent-interval slice-selective (QISS) MRA combined with MRI-based vascular calcification visualization for the assessment of arterial stenosis in patients with lower extremity peripheral artery disease. Eur Radiol. 2021;31(5):2778-2787.

142. Farber A, Menard MT, Conte MS, Kaufman JA, Powell RJ, Choudhry NK, Hamza TH, Assmann SF, Creager MA, Cziraky MJ, Dake MD, Jaff MR, Reid D, Siami FS, Sopko G, White CJ, van Over M, Strong MB, Villarreal MF, McKean M, Azene E, Azarbal A, Barleben A, Chew DK, Clavijo LC, Douville Y, Findeiss L, Garg N, Gasper W, Giles KA, Goodney PP, Hawkins BM, Herman CR, Kalish JA, Koopmann MC, Laskowski IA, Mena-Hurtado C, Motaganahalli R, Rowe VL, Schanzer A, Schneider PA, Siracuse JJ, Venermo M, Rosenfield K. Surgery or Endovascular Therapy for Chronic Limb-Threatening Ischemia. N Engl J Med. 2022;387(25):2305-2316.

143. Bradbury AW, Moakes CA, Popplewell M, Meecham L, Bate GR, Kelly L, Chetter I, Diamantopoulos A, Ganeshan A, Hall J, Hobbs S, Houlind K, Jarrett H, Lockyer S, Malmstedt J, Patel JV, Patel S, Rashid ST, Saratzis A, Slinn G, Scott DJA, Zayed H, Deeks JJ. A vein bypass first versus a best endovascular treatment first revascularisation strategy for patients with chronic limb threatening ischaemia who required an infra-popliteal, with or without an additional more proximal infra-inguinal revascularisation

procedure to restore limb perfusion (BASIL-2): an open-label, randomised, multicentre, phase 3 trial. Lancet. 2023;401(10390):1798-1809.

144. Rocha-Singh KJ, Zeller T, Jaff MR. Peripheral arterial calcification: prevalence, mechanism, detection, and clinical implications. Catheter Cardiovasc Interv. 2014;83(6):E212-220.

145. Fanelli F, Cannavale A, Gazzetti M, Lucatelli P, Wlderk A, Cirelli C, d'Adamo A, Salvatori FM. Calcium burden assessment and impact on drug-eluting balloons in peripheral arterial disease. Cardiovasc Intervent Radiol. 2014;37(4):898-907.

146. Roy T, Forbes T, Wright G, Dueck A. Burning Bridges: Mechanisms and Implications of Endovascular Failure in the Treatment of Peripheral Artery Disease. J Endovasc Ther. 2015;22(6):874-880.

147. Saba L, Sanagala SS, Gupta SK, Koppula VK, Johri AM, Khanna NN, Mavrogeni S, Laird JR, Pareek G, Miner M, Sfikakis PP, Protogerou A, Misra DP, Agarwal V, Sharma AM, Viswanathan V, Rathore VS, Turk M, Kolluri R, Viskovic K, Cuadrado-Godia E, Kitas GD, Sharma N, Nicolaides A, Suri JS. Multimodality carotid plaque tissue characterization and classification in the artificial intelligence paradigm: a narrative review for stroke application. Ann Transl Med. 2021;9(14):1206.

148. Iida O, Soga Y, Yamauchi Y, Hirano K, Kawasaki D, Tazaki J, Yamaoka T, Suematsu N, Suzuki K, Shintani Y, Miyashita Y, Takahara M, Uematsu M. Anatomical predictors of major adverse limb events after infrapopliteal angioplasty for patients with critical limb ischaemia due to pure isolated infrapopliteal lesions. Eur J Vasc Endovasc Surg. 2012;44(3):318-324.

149. Tavallaei MA, Zhou JJ, Roy TL, Wright GA. Performance Assessment of a Radiofrequency Powered Guidewire for Crossing Peripheral Arterial Occlusions Based on Lesion Morphology. Ann Biomed Eng. 2018;46(7):940-946.

9. Bibliography of the candidate's publications

Peer reviewed articles with relevance to the current work:

1. **Csőre J**, Suhai FI, Gyánó M, Pataki ÁA, Juhász G, Vecsey-Nagy M, Pál D, Fontanini DM, Bérczi Á, Csobay-Novák C. Quiescent-Interval Single-Shot Magnetic Resonance Angiography May Outperform Carbon-Dioxide Digital Subtraction Angiography in Chronic Lower Extremity Peripheral Arterial Disease. J Clin Med. 2022 Aug 1;11(15):4485. doi: 10.3390/jcm11154485. PMID: 35956102; PMCID: PMC9369435. **IF: 3.9**

2. Juhász G, **Csőre J**, Suhai FI, Gyánó M, Pataki Á, Vecsey-Nagy M, Pál D, Fontanini DM, Bérczi Á, Csobay-Novák C. A kontrasztanyag nélküli mágnesesrezonancia-angiográfia diagnosztikus teljesítménye alsó végtagi verőérbetegekben [Diagnostic performance of non-contrast magnetic resonance angiography in patients with lower extremity arterial disease]. Orv Hetil. 2022 Nov 6;163(45):1782-1788. Hungarian. doi: 10.1556/650.2022.32624. PMID: 36335484. **IF: 0.6**

3. **Csore J**, Karmonik C, Wilhoit K, Buckner L, Roy TL. Automatic Classification of Magnetic Resonance Histology of Peripheral Arterial Chronic Total Occlusions Using a Variational Autoencoder: A Feasibility Study. Diagnostics (Basel). 2023 May 31;13(11):1925. doi: 10.3390/diagnostics13111925. PMID: 37296778; PMCID: PMC10253011. **IF: 3.6**

4. **Csore J**, Drake M, Roy TL. Peripheral arterial disease treatment planning using noninvasive and invasive imaging methods. J Vasc Surg Cases Innov Tech. 2023 Aug 19;9(4):101263. doi: 10.1016/j.jvscit.2023.101263. PMID: 37767348; PMCID: PMC10520537. **IF: 0.7**

5. **Csore J**, Roy TL, Wright G, Karmonik C. Unsupervised classification of multi-contrast magnetic resonance histology of peripheral arterial disease lesions using a convolutional variational autoencoder with a Gaussian mixture model in latent space: A technical

feasibility study. Comput Med Imaging Graph. 2024 Mar 26;115:102372. doi: 10.1016/j.compmedimag.2024.102372. Epub ahead of print. PMID: 38581959. **IF: 5.7**

Other peer-reviewed articles:

1. Boga M, Suhai FI, Orbán G, Salló Z, Nagy KV, Szegedi L, Jokkel Z, **Csőre J**, Osztheimer I, Perge P, Gupta D, Merkely B, Gellér L, Szegedi N. Incidence and predictors of stroke and silent cerebral embolism following very high-power short-duration atrial fibrillation ablation. Europace. 2023 Nov 2;25(11):euad327. doi: 10.1093/europace/euad327. PMID: 37931067; PMCID: PMC10653180. **IF: 6.1**

2. Fontanini DM, Huber M, Vecsey-Nagy M, Borzsák S, **Csőre J**, Sótonyi P, Csobay-Novák C. Pulsatile Changes of the Aortic Diameter May Be Irrelevant Regarding Endograft Sizing in Patients With Aortic Disease. J Endovasc Ther. 2023 May 8:15266028231172368. doi: 10.1177/15266028231172368. Epub ahead of print. PMID: 37154393. **IF: 2.6**

3. Vecsey-Nagy M, Jermendy ÁL, Kolossváry M, Vattay B, Boussoussou M, Suhai FI, Panajotu A, **Csőre J**, Borzsák S, Fontanini DM, Csobay-Novák C, Merkely B, Maurovich-Horvat P, Szilveszter B. Heart Rate-Dependent Degree of Motion Artifacts in Coronary CT Angiography Acquired by a Novel Purpose-Built Cardiac CT Scanner. J Clin Med. 2022 Jul 26;11(15):4336. doi: 10.3390/jcm11154336. PMID: 35893427; PMCID: PMC9369248. **IF: 3.9**

4. Simon, J., Herczeg, S., Borzsák, S., **Csőre, J**., Kardos, A. S., Mérges, G., Zsarnóczay, E., Szegedi, N., Boussoussou, M., Vattay, B., Kolossváry, M., Szilveszter, B., Gellér, L., Merkely, B., & Maurovich-Horvat, P. (2022). Extracardiac findings on cardiac computed tomography in patients undergoing atrial fibrillation catheter ablation, Imaging, 14(1), 52-59. doi: 10.1556/1647.2022.00057 **IF: 0.4**

5. Vecsey-Nagy M, Jermendy ÁL, Suhai FI, Panajotu A, **Csőre J**, Borzsák S, Fontanini DM, Kolossváry M, Vattay B, Boussoussou M, Csobay-Novák C, Merkely B, Maurovich-Horvat P, Szilveszter B. Model-based adaptive filter for a dedicated

cardiovascular CT scanner: Assessment of image noise, sharpness and quality. Eur J Radiol. 2021 Dec;145:110032. doi: 10.1016/j.ejrad.2021.110032. Epub 2021 Nov 15. PMID: 34800835. **IF: 3.9**

6. Sarkadi H, Csőre J, Veres DS, Szegedi N, Molnár L, Gellér L, Bérczi V, Dósa E. Incidence of and predisposing factors for pseudoaneurysm formation in a high-volume cardiovascular center. PLoS One. 2021 Aug 24;16(8):e0256317. doi: 10.1371/journal.pone.0256317. PMID: 34428222; PMCID: PMC8384184. **IF: 3.752**

7. Simon J, Panajotu, A, **Csőre, J**, Pólos, Miklós, Zsarnóczay, Emese, Merkely B, Maurovich-Horvat P. Anomalous Left Coronary Artery Originating from the Right Coronary Sinus with an Interarterial Course: a Case Report and Literature Review Journal of Cardiovascular Emergencies, vol.6, no.2, 2020, pp.35-39. https://doi.org/10.2478/jce-2020-0005 **IF: -**

8. Kádár K, **Csőre J**, Liptai Cs, Tóth A, Kovács A, Molnár L, Suhai FI, Assabiny A, Kuthi, L, Édes I, Kertész AB, Merkely B, Hartyánszky I. Kawasaki-betegség gyermekkortól a felnőttkorig. Multimodális képalkotók szerepe a hosszú távú nyomonkövetésben CARDIOLOGIA HUNGARICA 47 : 4 pp. 243-249. , 7 p. (2017) **IF: -**

10. Acknowledgments

I would like to express my deepest gratitude to all those who have supported and contributed to the completion of my PhD thesis. Their unwavering guidance, encouragement, and assistance have been invaluable throughout this journey.

First and foremost, I am indebted to my supervisor, Csaba Csobay-Novák, for his exceptional mentorship, expertise, and patience. His insightful feedback, constructive criticism, and unwavering support have played a pivotal role in shaping my research and academic growth. I am truly grateful for his dedication and belief in my abilities.

I would also like to extend my appreciation to my supervisor in the Houston Methodist Hospital, Trisha L. Roy, for supporting me and guiding my work with her unparalleled expertise in PAD imaging, which significantly enriched my work.
I am especially grateful to Christof Karmonik for his guidance, which has been instrumental in shaping the direction and quality of this research.

I am immensely grateful to my colleagues and fellow researchers both in the Department of Radiology in the Heart and Vascular Center of Semmelweis University and the Houston Methodist Hospital, whose stimulating discussions and collaboration have provided a nurturing intellectual environment. Their support and friendship have been a constant source of motivation and inspiration.

I am deeply thankful to the technical staff and laboratory personnel who have provided invaluable assistance throughout my research. Their expertise, dedication, and willingness to share their knowledge have been invaluable in carrying out experiments, acquiring data, and troubleshooting various challenges.

I would like to express my heartfelt appreciation to my friends and family for their unwavering support, understanding, and encouragement throughout this demanding academic endeavor. Their love, belief in my abilities, and encouragement during both the highs and lows have been a constant source of strength.

DOI:10.14753/SE.2024.3024

To everyone who has played a part in this journey, directly or indirectly, I extend my sincere appreciation. Your contributions, no matter how small, have left an indelible mark on this work. I am forever grateful for the support, guidance, and encouragement that I have received, and I acknowledge that this achievement would not have been possible without the collective efforts of all those involved.

Thank you.